JAERI-Research
96-025

PERFORMANCE TEST OF LOWER HYBRID WAVEGUIDE UNDER LONG/HIGH-RF POWER TRANSMISSION

June 1996

Masami SEKI, Kenjiro OBARA, Sunao MAEBARA, Yoshitaka IKEDA
Tsuyoshi IMAI, Takashi NAGASHIMA, M. GONICHE*, J. BROSSAUD*
C. BARRAL*, G. BERGER-BY*, Ph. BIBET*, S. POLI*
G. REY* and G. TONON*

日本原子力研究所
Japan Atomic Energy Research Institute

本レポートは，日本原子力研究所が不定期に公刊している研究報告書です。
入手の問合わせは，日本原子力研究所技術情報部情報資料課（〒319-11 茨城県那珂郡東海村）あて，お申し越しください。なお，このほかに財団法人原子力弘済会資料センター（〒319-11 茨城県那珂郡東海村日本原子力研究所内）で複写による実費頒布をおこなっております。

This report is issued irregularly.
Inquiries about availability of the reports should be addressed to Information Division, Department of Technical Information, Japan Atomic Energy Research Institute, Tokai-mura, Naka-gun, Ibaraki-ken 319-11, Japan.

編集兼発行　日本原子力研究所
印　　刷　㈱原子力資料サービス

Performance Test of Lower Hybrid Waveguide under Long／High-RF Power Transmission

Masami SEKI, Kenjiro OBARA+, Sunao MAEBARA+, Yoshitaka IKEDA++
Tsuyoshi IMAI+, Takashi NAGASHIMA+, M. GONICHE*, J. BROSSAUD*
C. BARRAL*, G. BERGER-BY*, Ph. BIBET*, S. POLI*
G. REY* and G. TONON*

Department of Fusion Facility Division
Naka Fusion Research Establishment
Japan Atomic Energy Research Institute
Naka-machi, Naka-gun, Ibaraki-ken

(Received April 26, 1996)

Performance tests of a module for lower hybrid waveguides were carried out at the CEA Cadarache RF Test Facility. For the experiments the test module was fabricated by JAERI, the transmission line of the test bed was modified and the connection waveguides were manufactured by CEA.

As the results, the themal treatment by baking at a higher temperature was the most effective for reducing outgassing during injection of high RF power. The outgassing strongly depended on the temperature of the test module, but was independent to initial temperature. The RF injection reduced outgassing. The outgassing rate decreased to a low level of 10^{-6}-10^{-5} Pa m^3／sec m^2 (10^{-9}-10^{-8} Torr l／sec cm^2) at 400 ℃ after 450 ℃-baking. The gas injection did not affect outgassing before and during RF injection. The baking under H_2 or D_2 gas atmosphere were not so effective for reducing outgassing rete. The outgassing rate did not depend on input RF power densities.

The temperature in central part of the test module saturated to be ～100 ℃ by using of water cooling at a power level of 150 MW／m^2 RF injection, and a neutral gas pressure decreased gradually. In the water cooling case, the outgassing rate was very low less than 10^{-7} Pa m^3／sec m^2 (10^{-10} Torr l／sec cm^2). The steady state RF injection was demonstrated with water cooling.

Keywords: LHCD, Antenna, Waveguide, Steady-state Operation, Outgassing, Baking, Dispersion Strengthen Copper, High-RF Power, Heat Removal, Cooling

---

+ Department of Fusion Engineering Research
++ Office of Planning
* DRFC, Centre d'Etudes de Cadarache, CEA

長パルス・大電力伝送下での低域混成波アンテナ用導波管の評価試験

日本原子力研究所那珂研究所核融合装置試験部
関　正美・小原健治郎[+]・前原　直[+]
池田　佳隆[++]・今井　剛[-]・永島　孝[-]
M. GONICHE[*]・J. BROSSAUD[*]・C. BARRAL[*]・G. BERGER-BY[*]
Ph. BIBET[*]・S. POLI[*]・G. REY[*]・G. TONON[*]

（1996年4月26日受理）

低域混成波アンテナ用導波管のテストモジュールに対する評価試験が，フランス原子力庁カダラッシュ研究所の高周波試験施設にて実施された。試験用テストモジュールは原研が製作し，試験設備の伝送系の変更および接続導波管の製作をフランス原子力庁が行った。

ガス放出実験の結果によると，高周波入射中における導波管からのガス放出量の低減には，高温度ベーキングによる熱処理がもっとも効果的であった。ガス放出量はテストモジュールの温度に強く依存し，一方初期温度には依存しなかった。また，高周波入射もガス放出量の低減に役立つ。450度ベーキング処理を行った後のガス放出率は，400度において10^{-6}－10^{-5} Pa m^3／s m^{2}であった。高周波入射前および入射中のガス注入は，導波管からのガス放出量に影響を与えなかった。水素あるいは重水素中でのベーキングは，ガス放出量の低減には効果がなかった。ガス放出率は，高周波電力に依存しないことが確かめられた。

150 MW／m^{2}の高周波電力を入射中に水冷却することによって，テストモジュールの中央部での温度を100度程度に抑えることができ，ガス圧力も徐々に減少した。水冷却を用いて一定の低ガス放出率（～10^{-7} Pa m^3／s m^2）を観測し，連続入射の可能性を示した。

那珂研究所：311-01　茨城県那珂郡那珂町向山801－1
＋　核融合工学部
＋＋　企画室
＊　フランス原子力庁　カダラッシュ研究所

Contents

目　　次

1 INTRODUCTION

In the perspective of the tokamak reactor, it is an important issue to establish non-inductive current drive and active current profile control methods. Lower Hybrid Current Drive (LHCD) is an attractive candidate because it provides, so far, the highest current drive efficiency. The physical studies on LHCD have been performed on many tokamaks and the understanding of LHCD mechanism has been progressing. The data base for physical design of a next generation LHCD launcher is well documented by experiments on Asdex, JT-60, Tore Supra, JET, and others. However the data base for engineering design is not sufficient to plan a future LHCD launcher, especially in the case of steady state RF injection, and has to be improved.

For this data base, different topics are addressed such as: launcher mouth protection, disruption-induced stresses, RF splitting, optimization with respect of RF breakdowns... As far as steady state operation is concerned, it is crucial to estimate the outgassing rate of a launcher during RF injection, since a high gas pressure due to outgassing causes RF breakdowns and limits high power injection into the plasma. Recently the outgassing rate of prototype modules has been measured on test beds at Tore Supra [1], JET [2], and Tokamak de Varennes (TdeV) [3] for the prototype multijunction module of the 3.7 GHz LHCD launcher. The outgassing rate measured on Tore Supra and JET modules was relatively high, of the order of 10^{-4} Pa m^3 / sec m^2 (10^{-7} Torr. l / sec cm^2) at 300°C after baking at 230°C. On the other hand, the outgassing rate was two order lower in TdeV after a 450°C thermal treatment comparing to those of JET and Tore Supra. The outgassing rate of the launcher in JT-60 was estimated to be 10^{-6} Pa m^3 / sec m^2 (10^{-9} Torr l sec^{-1} .cm^{-2}), but temperatures in the whole launcher were not always measured. However these measurements were not sufficient for a quantitative data base. In particular, parameters governing the outgassing rate (pre-baking / working temperatures, RF power, RF aging, material...) were not fully established. In order to estimate the outgassing rate of waveguides correctly and to address the relevant parameters involved, a specific outgassing experiment was needed.

For this purpose, an exclusive test module was constructed by JAERI and the outgassing experiments with this module were carried out at the CEA Cadarache Test Facility, at a frequency of 3.7 GHz and a maximum power of 500 kW during quasi-continuous pulses. These outgassing experiments featured a low-temperature gradient in the test module comparing with former outgassing measurements performed at Tore Supra, JT-60, JET and TdeV: the tests were performed on a matched line terminated by a dummy load to avoid standing waves which produce inhomogeneity in temperature. In these experiments, we focused on searching effective thermal treatments, with the help of some basic theoretical models of the outgassing phenomena, to reduce the outgassing rate. We also demonstrated a steady state RF injection by using water cooling. Transient

outgassing due to breakdowns was not studied in details but can be found in the previous experiments [1]. Moreover for experiments on plasma, pressure rise in the waveguides can be also due to the interaction of the aperture of the antenna with the scrape-off layer plasma.

This report will describe the results of outgassing experiments. In section 2, the test module is described. The experimental set-up will be mentioned in section 3. The RF behavior of the test module is presented in section 4 while the outgassing experiment results are given in section 5. Section 6 discusses the results and a conclusion is drawn in the last section.

2. THE TEST MODULE

2.1 Design of the test module

The test module as shown in Fig. 1 is composed of three main parts: a set of 4 waveguides, cooling channels and connection flanges.

The key parameter governing outgassing rate in waveguides may be the working temperature, so that temperature uniformity is required for good determination of temperature dependence of outgassing. The height a of the waveguides was selected in order to have an uniform RF loss density on the surface of the waveguides: $a = \lambda_0 / 2^{0.5}$, where λ_0 is the wavelength in a free space. The schematic view of the waveguides and cooling channels is shown in Fig. 2. The general data of me module are given in the left column of appendix 1 .

The test module has cooling channels on the both H-planes (small sides of the waveguides) to insure the lowest thermal gradient during RF injection. The cooling route is sketched in Fig. 3. A schematic drawing of the cooling channels is given in Fig. 4. These cooling channels are also used to perform temperature control of waveguide during a long pulse.

In order to have a low pressure gradient, pumping holes of 4 mm diameter are machined in the 5 walls of the module, with a spacing of ~$\lambda g/4$, yielding to a total effective conductance of 0.09 m^3 / sec (for N_2 at 20°C).

RF contact between the test module and the connection waveguide is one of the important issues of this experiment in-vacuum at high temperature. This RF contact must transmit high RF power without breakdown after high temperature baking up to 450°C. For the test module a metal o-ring is used as the RF contact, it was the metal joint made of Ag-gilded stainless steel which showed availability up to 250°C baking in the JT-60 LHCD launcher. Moreover, a silver-based solution was sprayed on the septa of the test

outgassing due to breakdowns was not studied in details but can be found in the previous experiments [1]. Moreover for experiments on plasma, pressure rise in the waveguides can be also due to the interaction of the aperture of the antenna with the scrape-off layer plasma.

This report will describe the results of outgassing experiments. In section 2, the test module is described. The experimental set-up will be mentioned in section 3. The RF behavior of the test module is presented in section 4 while the outgassing experiment results are given in section 5. Section 6 discusses the results and a conclusion is drawn in the last section.

2. THE TEST MODULE

2.1 Design of the test module

The test module as shown in Fig. 1 is composed of three main parts: a set of 4 waveguides, cooling channels and connection flanges.

The key parameter governing outgassing rate in waveguides may be the working temperature, so that temperature uniformity is required for good determination of temperature dependence of outgassing. The height a of the waveguides was selected in order to have an uniform RF loss density on the surface of the waveguides: $a = \lambda_0 / 2^{0.5}$, where λ_0 is the wavelength in a free space. The schematic view of the waveguides and cooling channels is shown in Fig. 2. The general data of me module are given in the left column of appendix 1 .

The test module has cooling channels on the both H-planes (small sides of the waveguides) to insure the lowest thermal gradient during RF injection. The cooling route is sketched in Fig. 3. A schematic drawing of the cooling channels is given in Fig. 4. These cooling channels are also used to perform temperature control of waveguide during a long pulse.

In order to have a low pressure gradient, pumping holes of 4 mm diameter are machined in the 5 walls of the module, with a spacing of ~$\lambda g/4$, yielding to a total effective conductance of 0.09 m^3 / sec (for N_2 at 20°C).

RF contact between the test module and the connection waveguide is one of the important issues of this experiment in-vacuum at high temperature. This RF contact must transmit high RF power without breakdown after high temperature baking up to 450°C. For the test module a metal o-ring is used as the RF contact, it was the metal joint made of Ag-gilded stainless steel which showed availability up to 250°C baking in the JT-60 LHCD launcher. Moreover, a silver-based solution was sprayed on the septa of the test

module to insure low RF losses around the mouth after re-machining as shown in Fig. 5.

Concerning the material, the test module should have the following properties; I) high-electrical conductivity for reducing RF loss, 2) high-thermal conductivity for baking and cooling, 3) high-strength at high temperature for avoiding deformation of waveguides and 4) low-outgassing rate for obtaining good vacuum. For the waveguides septa, dispersion strengthened copper (DSC) is adopted because it has the properties of 1) - 3), and should have the properly of 4) according to the previous results [3]. On the other hand the electrical resistance of the module has to be high enough to reduce the strength of the induced eddy current when a plasma disruption occurs. For this purpose, stainless steel is selected as the material for the spacer between the DSC plates and for the cooling channels. This structure with two different materials has already been proposed by JAERI in ITER-CDA design [4].

2.2. Fabrication of the test module

To obtain a high current drive efficiency in the LHCD experiments, many waveguides are needed for launching an optimized spectrum with a narrow peak and high directivity. The waveguides must be fabricated with good accuracy without deformation in order to maintain the designed RF properties. For these requests, a diffusion bonding method has been developed through the fabrication of a multijunction launcher in JT-60U. The 24 waveguides of the launcher were bonded by diffusion process between copper-plated stainless steels (CSS) in a hot isostatic press machine.

This diffusion bonding method is applied to fabricate the waveguides composed of two different materials as mentioned in 2.1 section. Conditions for the diffusion bonding of DSC-CSS are optimized. Finally, the test module is fabricated under the following conditions :

- H_2 atmosphere,
- pressure of 10 MPa (100 kg / cm^2),
- temperature of 850°C for 2 hours.

The development of this fabrication technique for a launcher by diffusion bonding process can be found in ref. 5. The cooling channels are installed on the waveguides by an Ag-brazing method as shown in Fig. 2. Figure 6 shows the vacuum tight connection of the cooling pipes. No special pre-treatment is performed, but the test module is washed with an acetone solution. The photograph of Fig. 1 shows an overview of the test module. In the course of fabrication of the test module, the pressing on the test module is unbalanced, so that heights of the module are deformed from the design value. The height of the waveguides is a very important parameter for the RF properties (see section 4) since it determines the phase of the propagating wave. Before the high-power experiment, the heights are measured at each end of the waveguides (design value is

57.3 mm in Fig. 5). After the experiment is completed, the heights are measured all along the module. The following remarks can be done :

- very close values are found before and after experiment at each end,
- differences in height between wg 1 and 2 (open symbols of Fig. 7) and wg 3 and 4 (closed symbols) just occur at the very end of the module,
- the high profile a (z) is the same for the four waveguides on most of the length with a maximum deviation from the design value (57.3 mm) of 1.3 mm and 2.1 mm for wg 3 - 4 and wg 1 - 2, respectively.

However after experiments, a distortion of the central septum is noticed as shown in Fig. 8. This plastic deformation has no significant effect on the waveguides height and the RF properties of the module.

3. THE EXPERIMENTAL SET-UP

3.1. Outline

The outgassing experiments on the test module are performed at the CEA Cadarache Test Facility. No short plate at the waveguides end is adopted under high-power tastes in order to avoid standing wave that provides temperature gradient along the waveguides. The test bed is modified to adjust the transmission line to the test module. The two connection waveguides are prepared by CEA. A photograph of the experimental set-up is shown in Fig. 9.

A schematic of the experimental set-up is drawn in Fig. 10. A klystron produces a high-RF power up to 500 kW at a frequency of 3.7 GHz quasi continuously (see appendix 2). The RF power is transmitted from the klystron to the input RF window via the WR-284 waveguides of the 8.4 m long transmission line and from the output RF window to a water dummy load via a 12.2 m long transmission line. These transmission lines have cooling pipes for continuous operation and are filled with SF6 gas for avoiding breakdowns. A bellow at downstream side of the chamber is used as an absorber for thermal expansion as shown in Fig. 11. Where the initial temperature is 20°C and the maximum final temperature is 500°C, the thermal expansion length is 11 mm.

3. 2. The connection waveguides

The connection waveguides are two non-divided waveguides, of length L = 0.765 m, are provided to connect the module to the input and output RF windows. These parts are made of copper zirconium (0.15 %) plates for the waveguides. Rods for the cooling

57.3 mm in Fig. 5). After the experiment is completed, the heights are measured all along the module. The following remarks can be done :

- very close values are found before and after experiment at each end,
- differences in height between wg 1 and 2 (open symbols of Fig. 7) and wg 3 and 4 (closed symbols) just occur at the very end of the module,
- the high profile a (z) is the same for the four waveguides on most of the length with a maximum deviation from the design value (57.3 mm) of 1.3 mm and 2.1 mm for wg 3 - 4 and wg 1 - 2, respectively.

However after experiments, a distortion of the central septum is noticed as shown in Fig. 8. This plastic deformation has no significant effect on the waveguides height and the RF properties of the module.

3. THE EXPERIMENTAL SET-UP

3.1. Outline

The outgassing experiments on the test module are performed at the CEA Cadarache Test Facility. No short plate at the waveguides end is adopted under high-power tastes in order to avoid standing wave that provides temperature gradient along the waveguides. The test bed is modified to adjust the transmission line to the test module. The two connection waveguides are prepared by CEA. A photograph of the experimental set-up is shown in Fig. 9.

A schematic of the experimental set-up is drawn in Fig. 10. A klystron produces a high-RF power up to 500 kW at a frequency of 3.7 GHz quasi continuously (see appendix 2). The RF power is transmitted from the klystron to the input RF window via the WR-284 waveguides of the 8.4 m long transmission line and from the output RF window to a water dummy load via a 12.2 m long transmission line. These transmission lines have cooling pipes for continuous operation and are filled with SF6 gas for avoiding breakdowns. A bellow at downstream side of the chamber is used as an absorber for thermal expansion as shown in Fig. 11. Where the initial temperature is 20°C and the maximum final temperature is 500°C, the thermal expansion length is 11 mm.

3. 2. The connection waveguides

The connection waveguides are two non-divided waveguides, of length L = 0.765 m, are provided to connect the module to the input and output RF windows. These parts are made of copper zirconium (0.15 %) plates for the waveguides. Rods for the cooling

pipes are assembled by brazing with the same technique as was used for the Tore-Supra antennae modules[1]. A $\lambda_g/4$ step transformer is machined in the flange to adapt the impedance of the test module, of height 57.3 mm, for the impedance of the connection waveguide, of height 76.0 mm as shown in Fig. 12 and 13.

From the calculation of RF losses, it is estimated that the temperature rise would be smaller by a factor of 5 with respect of the test module and outgassing of these connections is expected be negligible compared with that from the test module. Details on these connections are given in the right column of appendix 1.

3.3 The pumping system

The volume and the surface of the vacuum chamber are 0.146 m^3 and 3.11 m^2, respectively. The vacuum chamber has a pumping unit composed of a turbo molecular pump of 0.5 m^3 / s and a rotary pump of 0.33 m^3 / min. The measured effective pumping speed is 0.23 m^3 / s for H_2. A mass spectrometer is installed on an additional chamber with its own pumping unit (~ 0.2 m^3 / s) and connected to the main chamber by a rather low conductance (0.01 m^3 / s) pipe.

3.4 Baking and cooling systems

A baking system is used to heat the vacuum chamber up to 450°C. This system is feedback controlled by monitoring the temperature of the chamber. The test module and the connection waveguides are heated mainly by radiation from the chamber. However a large temperature gradient along the 2.3 m long chamber is necessary to maintain a temperature of 150°C at two flanges where viton o-rings are used for vacuum seal.

Before installation of the test module, the vacuum chamber of the test bed, made of stainless steel, is baked at the maximum temperature of 450°C. Time evolution of the pressure and the temperature during a baking cycle is shown in Fig. 14. The different baking cycles reduced significantly the outgassing rate of the tank to 10^{-8} Pa m^3 / s m^2 (~10^{-11} Torr l /.s.cm^2) at room temperature as shown in Fig. 15.

Cooling of the test module and the connection waveguides is performed by water or air flow. Air cooling is manly used to restore a low initial temperature before RF injection (T < 200°C) and water cooling to obtain a steady state temperature during long RF injection.

At higher power level (P > 200 MW / m^2), the cooling of the directional couplers, by the water flow and by direct air venting, is not sufficient and then the RF pulse length has to be limited up to 3 min.

3.5 RF measurement

The RF measurements are performed by directional couplers at three locations in the transmission line as shown in Fig. 16.

- At the klystron output :
  incident power P_i^k (this measurement is also used for klystron power control),
  reflected power P_r^k for a fast RF switch off system

- At the test module input :
  incident power P_i^m
  incident phase Φ_i^m
  reflected power P_r^m

- At the test module output :
  incident power $P'_i{}^m$
  incident phase $\Phi'_i{}^m$
  reflected power $P'_r{}^m$

RF signals are processed and sent to me data acquisition system. From calorimetric measurements of the transmission lines losses (~ 15 %) and of the power dumped into the matched load, it is deduced that the RF powers at the klystron and test module outputs are overestimated by 10 % and 7 %, respectively as shown Fig. 17. After high power (150 MW / m^2) long pulses, the directivity of the couplers at the input and the output of the module is degraded and power values have to be corrected by a factor of 1.1 and 1.2, respectively.

3.6 Temperature measurement

Fourteen thermocouples (10 for the test module and 4 for the connections) under vacuum are available. One of the thermocouples attached to the chamber is used to feedback-control the baking temperature.

The inlet and outlet temperature of the cooling water are measured for a calculation of RF losses. The same kind of measurements are made to calculate the power dumped into the load.

3.7 Pressure and outgassing measurements

In order to measure the outgassing flux, two ionization gauges are available. Gauge 1 is used on a linear scale and gauge 2 on a logarithmic scale. For partial pressure, the mass spectrometer, installed in the secondary tank, is calibrated for different gases : H_2, D_2, CH_4, N_2, Ar. Calibration for H_20, CO and CO_2 is deduced. Mass spectrometer failed during experiments and is replaced by a more rough system (QMG 064) with no electron multiplier. All calibrations are done from the ionization gauge signal giving "N2 equivalent" pressure as shown in Fig. 18. It is verified that the addition of the 4 main partial pressures (H_2, H_2O ,CO, CO_2) is consistent with the measurement of total pressure during an outgassing experiment as shown in Fig. 19. A discrepancy (~50 %) is only found in the low pressure range. Ionization efficiency is then taken into account for the calculation of the actual partial pressure whereas no correction is made for the total pressure and total outgassing flux.

Before RF injection, outgassing flux is measured by closing the valve of the pumping unit (build-up method). The slope of pressure rise (dP / dt) gives the total outgassing Q of the system composed of the tank, the connection waveguides and the test module:

$$Q = V \cdot dP / dt, \qquad (1)$$

where V is the volume of the tank.
During RF injection, outgassing flux is calculated from the dynamic equation :

$$Q = V \cdot dP / dt + S \cdot P, \qquad (2)$$

where S is the effective pumping speed in the tank.

It is assumed that time evolution of outgassing of the tank and the connection waveguides is negligible. Contribution of these parts, Qw, is experimentally deduced as follows : Outgassing flux of the test module Q-Qw is plotted as a function of 1/T on a semi-log scale. By adjusting Qw, a straight line can be obtained as shown in Fig. 20. Depending upon the initial temperature T_0, Qw lies between $2x10^{-6}$ and $1x10^{-5}$ Pa m^3 / s. Error bars with this method is estimated to be +/- $1x10^{-6}$ Pa.m^3 / s for the outgassing flux Q (i.e. $1x10^{-6}$ Pa.m^3 / s m^2 for the outgassing rate q) and leads to large errors when the outgassing flux is low. In order to have a better accuracy, the build-up method is also used from shot # 822 for the measurement of outgassing rates. When Qw is about twice the outgassing of the test module (i.e. when pressure increases by a factor of 1.5), the build-up method leads to an outgassing flux lower by a factor of 1 to 5.

For the outgassing rate q, we will consider the average rate of the module :

$$q = (Q - Qw) / Smod, \quad (3)$$

where Smod is surface area of the test module.

3.8 Control and acquisition data system

The klystron is controlled by a wired electronics. A security system protects the klystron when an interlock signal (RF reflected power, pressure in tube of klystron, temperature in cavity, temperature in collector cooling water) is detected. For the reflected power, the threshold is set to 20 kW.

Measurements of the 46 signals are gathered by a desk computer. These measurements include the klystron parameters, temperatures of the load and transmission line (calorimetric), the RF powers, the neutrals pressures in the vacuum tank, the temperatures of the module and the connection waveguides.

A software allows to display the calibrated measurements and derives values such as the RF losses and the outgassing fluxes. The acquisition data rate is in the range of 0.2 s (for RF measurements) to 1.0 s (for temperature measurements). The acquisition data flow is typically 1 Mbytes for a long shot.

4. RF PROPERTIES OF THE TEST MODULE

4.1 VSWR of the test module

VSWR of the test module, with tapered waveguides, was firstly measured : at 3 .7 GHz, the value is 1 .31. The test module is then installed in the test bed and VSWR is measured from input RF window to the dummy load. This test includes connections waveguides, RF windows and the down stream transmission line : in the 3.695-3.705 GHz band, VSWR is lower than 1.25 (1.15 at 3.7GHz) as indicated in Fig. 21. After the experimental campaign is completed, VSWR of the test module, the connection waveguides and the input RF window is measured: in the 3.695-3.705 GHz band, VSWR is lower than 1.22 (1.13 at 3.7 GHz) as indicated in Fig. 22. These low values allow high power test with safe operation of the klystron which can withstand a VSWR of 1.34 at the nominal power of 500 kW (1.54 at 400 kW). Due to the difference in the experimental set-up, no conclusions can be drawn on a possible plastic distortion of the test module due to the high temperature heating during the high power tests. However

For the outgassing rate q, we will consider the average rate of the module :

$$q = (Q - Qw) / Smod, \quad (3)$$

where Smod is surface area of the test module.

3.8 Control and acquisition data system

The klystron is controlled by a wired electronics. A security system protects the klystron when an interlock signal (RF reflected power, pressure in tube of klystron, temperature in cavity, temperature in collector cooling water) is detected. For the reflected power, the threshold is set to 20 kW.

Measurements of the 46 signals are gathered by a desk computer. These measurements include the klystron parameters, temperatures of the load and transmission line (calorimetric), the RF powers, the neutrals pressures in the vacuum tank, the temperatures of the module and the connection waveguides.

A software allows to display the calibrated measurements and derives values such as the RF losses and the outgassing fluxes. The acquisition data rate is in the range of 0.2 s (for RF measurements) to 1.0 s (for temperature measurements). The acquisition data flow is typically 1 Mbytes for a long shot.

4. RF PROPERTIES OF THE TEST MODULE

4.1 VSWR of the test module

VSWR of the test module, with tapered waveguides, was firstly measured : at 3 .7 GHz, the value is 1 .31. The test module is then installed in the test bed and VSWR is measured from input RF window to the dummy load. This test includes connections waveguides, RF windows and the down stream transmission line : in the 3.695-3.705 GHz band, VSWR is lower than 1.25 (1.15 at 3.7GHz) as indicated in Fig. 21. After the experimental campaign is completed, VSWR of the test module, the connection waveguides and the input RF window is measured: in the 3.695-3.705 GHz band, VSWR is lower than 1.22 (1.13 at 3.7 GHz) as indicated in Fig. 22. These low values allow high power test with safe operation of the klystron which can withstand a VSWR of 1.34 at the nominal power of 500 kW (1.54 at 400 kW). Due to the difference in the experimental set-up, no conclusions can be drawn on a possible plastic distortion of the test module due to the high temperature heating during the high power tests. However

VSWR remains at a low value. During the high power tests, VSWR is also measured : at the input RF window, with an incident power of 150 kW power, the reflected power increased from 1.5 kW (VSWR ~1.2), at 100°C to 10 kW (VSWR ~1.65), at 500°C, as indicated in Fig. 17. VSWR at low temperature value is in good agreement with the low power level measurement whereas the high temperature measurement indicates some elastic distortions of the test module which enhance the reflection.

4.2 RF losses

RF losses of the test module and the connection waveguides are estimated from thermometry of the walls. RF losses heat up adiabatically the waveguides walls at a constant rate dT / dt . In zero-dimensional model, the losses per unit of length, P_{loss} is determined from the relation :

$$P_{loss} = m_0 c_p \, dT / dt, \qquad (4)$$

where m_0 is the mass per unit of length of the considered waveguides section and c_p specific heat (see appendix 1). P_{loss} is experimentally determined from relation (4) and compared to the theoretical value Pth given by :

$$Pth = 0.3206 \, \rho^{0.5} \, [\, 2(a+b) - 2(\, 1-\lambda_0^2 / 2a^2) \,] \, / \, (\, 1-\lambda_0^2 / 4a^2)^{0.5} \times P_{rf}, \qquad (5)$$

where ρ is the electrical resistivity which depends on the temperature (appendix 1) and P_{rf} the power density of the RF wave as RF power divided by cross section of a x b (a > b). In the test module, height of waveguide is specified as $a = \lambda_0 / 2^{0.5}$ and the RF losses are homogeneous all along the perimeter of the waveguides.

Figure 23-a shows the measured RF losses at different RF powers for the test module (L = 1.0 m) and the connection waveguides (L = 2 x 0.765 m). The experimental values Ploss of ~2.4 % for the module and 0.7 % for the connections fit the calculation ones Pth within 15 %. Global losses of the test module and connections are estimated by calorimetry when the whole system is water cooled (flow rate: 0.21 kg/s) : a reasonable accordance is found between the experimental and the calculated values at different powers as shown in Fig. 23-b.

4.3 Resonant phenomena

At high temperature, an anomalous heating rate is observed at some location of the test module as shown in Fig. 24. Six thermo-couples are installed on the test module. The thermo-couple are named as Tmodule 1-6. Tmodule 1, 3, 5 are set on wg 1 at periphery of E-plane and Tmodule 2, 4, 6 are set on wg 4 at center of E-plane. The heating rate of Tmodule 5 increases by a factor of l 1, from 0.9 to 10°C / s, whereas Tmodule 3 at a distance of 380 mm (= 3.3 λg ~ (3+1/4) λg) cools down. This longitudinal modulation indicates that the surfaces are heated by RF losses due to a standing wave excited. These enhanced losses are accompanied by a strong RF power absorption evaluated as the difference between the incident powers measured by the output and input couplers. This phenomena strongly depends on the power level : at 50 MW / m^2, power absorption only increases by 30 % from 3 to 4 kW. But it increases by a factor 6, from 8 to 50 kW, at a power density level of 150 MW / m^2 (270 kW) as shown in Fig. 25. This phenomena is interrupted that the reflected power increases at outlet of the test module due to thermal expansion, and multi-reflection occurs in the test module such as resonant cavity.

The sensitivity of the RF behavior of the test module to the four waveguides height is tested by computing the scattering matrix of the test module with height and length of the sub-waveguides as input parameters. Due to thermal expansion, the length is assumed to be time-dependent but the heights are supposed to be constant. When the height of wg 3 and 4 differs from the height of wg 1 and 2 by only 0.1 mm, power absorption increases from 4 to 10.5 % at T = 400°C as illustrated in Fig. 26. This result is qualitatively consistent with experimental values. However the power dependence, indicating distortion of the height during the RF injection, is not taken into account. Basically this resonance occurs due to the symmetric structure of the test module in longitudinal direction because of the strong inter-coupling between sub-waveguides at the inlet and outlet junctions. In a non-symmetric waveguide such an antenna module for launching power to a plasma, such a resonant phenomena would not occur.

4.4 High power handling capability

After first installation of the test module, RF performance is checked without previous baking. Conditioning of the test module is achieved by short pulses (10ms) sequences and then by 3 to 10 s pulses. After 1500 short RF pulses, level of 50 MW / m^2 (90 kW of injected power) is attained. Then sixty long pulses of 3 sec are needed to perform a breakdown free pulse at the same power level as shown in Fig. 27. Following the first thermal treatment (300°C / 60 hours), a power level of 90 kW is quite easily restored after 30 pulses of 10 s duration. Higher power densities (100, 150 and 200 MW / m^2) are all obtained with even shorter conditioning phase as indicated in appendix 3. It

should be pointed out that conditioning effect is never lost after air exposure of 12 hours proceeding a thermal treatment and that the level of 50 MW / m^2 could be obtained at the first shot without RF aging. Long pulses of 5 min are obtained just after conditioning phase. Conditioning at 200 MW / m^2 level is achieved at late phase of this outgassing experiments, at this recorded power level, breakdown-free RF injections are easily obtained as illustrated in Fig. 28.

It should be noticed that a good RF contact is maintained all along the RF injections up to a temperature of 450°C at the flanges for 50 MW / m^2 and 350°C for 150 MW / m^2. However some spots are observed on the contact surface of the test module and connection waveguides flanges as shown in Fig. 8.

5. OUTGASSING EXPERIMENTS

5.1 Experimental procedure

5.1.1 Thermal pre-treatment

Four types of thermal pre-treatment are performed at medium / high temperature and with / without hydrogen gas as follows.

Treatment 1 and 2:	300°C / 60 hours ; this treatment is reproduced after an air leak
Treatment 3:	300°C / 60 hr including 10 hr with hydrogen gas of 10 Pa
Treatment 4:	400°C / 45 hr + 450°C / 10 hr
Treatment 5:	400°C / 50 hr + 450°C / 8 hr with deuterium gas of 10 Pa.

5.1.2 Initial outgassing of the total system

It is expected that outgassing depends on initial conditions of the surface molecules coverage and therefore on initial outgassing Q_0 (see section 6). Global initial outgassing of the total system is measured before each RF injection. This initial outgassing strongly depends on temperature as shown in Fig. 29. The initial outgassing at 200°C seems to have reduced significantly by a factor of 3 after the last baking of 450°C in deuterium atmosphere.

5.1.3 Experimental parameters

should be pointed out that conditioning effect is never lost after air exposure of 12 hours proceeding a thermal treatment and that the level of 50 MW / m^2 could be obtained at the first shot without RF aging. Long pulses of 5 min are obtained just after conditioning phase. Conditioning at 200 MW / m^2 level is achieved at late phase of this outgassing experiments, at this recorded power level, breakdown-free RF injections are easily obtained as illustrated in Fig. 28.

It should be noticed that a good RF contact is maintained all along the RF injections up to a temperature of 450°C at the flanges for 50 MW / m^2 and 350°C for 150 MW / m^2. However some spots are observed on the contact surface of the test module and connection waveguides flanges as shown in Fig. 8.

5. OUTGASSING EXPERIMENTS

5.1 Experimental procedure

5.1.1 Thermal pre-treatment

Four types of thermal pre-treatment are performed at medium / high temperature and with / without hydrogen gas as follows.

Treatment 1 and 2:	300°C / 60 hours ; this treatment is reproduced after an air leak
Treatment 3:	300°C / 60 hr including 10 hr with hydrogen gas of 10 Pa
Treatment 4:	400°C / 45 hr + 450°C / 10 hr
Treatment 5:	400°C / 50 hr + 450°C / 8 hr with deuterium gas of 10 Pa.

5.1.2 Initial outgassing of the total system

It is expected that outgassing depends on initial conditions of the surface molecules coverage and therefore on initial outgassing Q_0 (see section 6). Global initial outgassing of the total system is measured before each RF injection. This initial outgassing strongly depends on temperature as shown in Fig. 29. The initial outgassing at 200°C seems to have reduced significantly by a factor of 3 after the last baking of 450°C in deuterium atmosphere.

5.1.3 Experimental parameters

Seventy five shots are achieved with RF injection duration ranging between 1 and 101 min, with most of the shots between 5 and 30 min.

Outgassing experiments are run with three initial temperatures : 200°C (35 shots), 100°C (15 shots) and 20°C (25 shots). For the first shot of the day, temperature gradient of the test module is very small, but the air cooling system can not remove the heat homogeneously and down stream region is hotter than upper stream by almost 60°C for the worse case.

Dependence of outgassing flux on temperature of the test module is studied and reduction in outgassing by baking is investigated. Effect of power level on outgassing flux is tested, influence of deuterium gas puffing (20 shots) before and during RF injection is also examined. In order to obtain thermal equilibrium of the test module, air (11 shots) and water cooling (13 shots) are used.

A data base has been established from the 75 shots indicating the main parameters and the outgassing flux at T =200, 300, 400 and 500°C.

5.2 Experimental results

5.2.1 Time evolution of pressure

As already observed during the previous experiments on Tore Supra prototype module[1] and TdeV prototype module[2], the pressure increases quasi exponentially during RF injection. However for the first long pulse injection (50 MW / m^2 - 5 min.), pressure just increases by a factor of 2 as illustrated in Fig. 30. During the ramp-up phase of the power, three breakdowns occurs. However the pressure recovers its initial value in less than 10 s. Total amount of gas desorbed per one breakdown is 1.5 x 10^{-5} Pa m^3 which is only a factor of 2 larger than the previous measurements on Tore-Supra test module.

Because of this slow evolution of the pressure, the pulse duration is extended to the maximum compatible with safe operation : power is switched off when the maximum temperature reaches 500°C. However, even for these very long pulses up to 101 min, saturation of the pressure is never observed. This point will be discussed in section 6. To focus on temperature dependence of outgassing flux Q, a semi-log plot of Q versus 1 / T is used. Such a curve shows a linear dependence up to 400-450°C like a Fig. 31 and the slope can be interpreted as the activation energy of the desorption phenomena (see section 6). Outgassing flux in higher temperature > 450°C increases even faster. This can be related to another mechanism of desorption or desorption coming from the connection waveguides.

5.2.2 Residual gases composition

During the RF injection, residual gas composition is evaluated from measurement of ratio Pi / Ptotal (i = H_2, H_2O, CO, CO_2). Although the total pressure increases by almost two orders of magnitude, this ratio is fairly constant for H_2O, CO and CO_2, until temperature of the test module reaches 400°C as shown in Fig. 32. Only an increase of hydrogen concentration is observed from 16 to 26 % at 370°C while CO and CO_2 concentration slightly decreases. CO and CO2 concentration increases > 400°C and 50 % of the desorbed species is CO_2 molecules at 500°C. The main desorbed gas is hydrogen (~ 60 %) when breakdowns occur.

Total and partial outgassing flux is indicated as a function of 1 / T in Fig. 33. As known from the figure, the slopes for the four main outgassing fluxes are close. On the other hand a large increase of the partial pressure is observed above 420°C for H_2O, CO, CO_2 exception of H_2.

5.2.3 RF power dependence

To evaluate the RF power dependence on outgassing rate, RF powers are injected into the test module at different power levels (50, 100, 150 MW / m^2). The outgassing rates Q are compared by plotting Log Q as a function of 1 / T as shown in Fig. 34. Very close curves for the 3 powers are obtained with the same slope (E_d = 0.40 eV) and the same trend to further increase over T ~ 450°C. A statistical analysis of 70 shots confirms this result. The outgassing rate measured at T = 400°C shows a large scattering due to the different conditioning state, but no power dependence as illustrated in Fig. 35.

5.2.4 Evolution of outgassing with aging and thermal treatment

Outgassing has been systematically analyzed at T = 300, 400 and 500°C with the 55 available shots. As already observed, the outgassing rate decreases shot by shot. In this experiment, the temperature of 500°C is routinely reached, the baking effect provided by RF losses is strong. The test module is baked above 300°C, which is the first baking temperature, during ~50 % of the R F injection time. A relevant parameter to characterize this baking effect is the integrated injected energy which is proportional to the integrated absorbed energy by the test module (RF loss ~ 3.5 %). Figures 36, 37 and 38 show the outgassing flux measured at 300, 400 and 500°C respectively as a function of the integrated energy. The first shot after a thermal treatment is plotted with a closed circle.

The largest outgassing flux Q measured is $5x10^{-3}$ Pa.m^3 / s (q ~ $5x10^{-3}$ Pa.m^3 / s m^2) at the end of the first very long pulse with 500°C. This large outgassing is never obtained again even after air exposure. The first shot after air exposure and thermal treatment has a higher outgassing rate. A strong decrease in the outgassing rate is later obtained, particularly for the first series where the outgassing rate at 400°C decreases by almost two orders of magnitude to values in the 10^{-6} Pa.m^3 / s m^2 range. Higher temperature baking at 450°C is also efficient for reducing the outgassing rate at high temperature (400 and 500°C) by a factor 2 to 10.

In measurement of outgassing rate below 10^{-5} Pa.m^3 / s m^2, the dynamic method leads to large error bars and the a build-up method is useful. The data measured by a build-up method show a small scattering as shown in Fig. 39 and an "ultimate" outgassing rate Qult can be given :

Qult ~ $2x10^{-7}$ Pa.m^3 / s m^2 at T = 300°C
Qult ~ $6x10^{-7}$ Pa.m^3 / s m^2 at T = 400°C

Thermal treatments in H_2 or D_2 atmosphere have no significant effect on global outgassing. After baking at 450°C with deuterium, mass spectrometry indicates that a large amount of deuterium is outgassed, specially involved in HDO and D_2O molecules as shown in Fig. 40. This deuterium is observed all along the last series of shots. Isotopic ratio D / D+H evaluated with m / e = 2, 3, 4, 18, 19, 20 peaks decreases from 40 % (shot # 945) to 20 % (shot # 1084). Hydrogen-like molecules content remain rather low ($P_{H2} + P_{D2}$) / Ptotal = 30 %.

5.2.5 Effect of gas puffing

In order to reproduce the scenario of RF injection during a plasma shot, gas puff of deuterium is performed before switching on RF. The time delay between gas puffing and RF injection is about 20 s. The deuterium gas puffing is also performed during the RF injection. The maximum pressure is about 10^{-2} Pa. Deuterium gas is indeed immediately pumped out by the pumping system and no further desorption of deuterium is measured in both cases as shown in Fig. 41 even at the onset of the power where an increase of H_2 pressure is only observed.

Moreover, at least up to 100 MW / m^2, no breakdown occurs despite the pressure increases and the reflected power as well as the incident phase at the output of the test module vary very little as shown in Fig. 42 (on a time scale of 0.6 s which is the acquisition data rate for the shot). The pumping time constant for deuterium is 0.7 sec.

5.2.6 Control of the temperature rise rate

Without active cooling, the temperature increases linearly with time. By cooling the test module and the connection waveguides with an air flow rate of 700 N l / min, the temperature rise rate is reduced from 0.3°C / s to 0.025°C / s as shown in Fig. 43 in the case of injection at 50 MW / m^2. This allows, for this power level, to extend the RF injection duration from 32 min to 101 min with initial temperature Ti = 20°C until the maximum temperature reaches 500°C as illustrated in Fig. 44. Air cooling has also an effect on the temperature profile as shown in Fig. 45. Heat exchanges in down stream is not sufficient because of short cooling channel due to lack of space in the vacuum chamber. However an Arrhenius plot log Q vs 1 / T shows a similar temperature dependence of the outgassing with a larger outgassing by a factor of 3 at T = 500°C as shown in Fig. 46. This large outgassing can be explained by a higher temperature of the down stream section of the test module. The outgassing flux Q at 500°C is around $5x10^{-6}$ Pa m^3 / s (q ~ $3x10^{-6}$ Pa m^3 / s m^2).

5.2.7 Stationary outgassing

Long RF injection is performed from room temperature with water cooling of the test module at flow rate of 12.5 l / min. Quasi-stationary temperatures are obtained all along the test module and the connection waveguides up to a power level of 150 MW / m^2 after 30 min of RF power injection as shown in Fig. 47. The largest temperature rise rate at the down stream section is about $5x10^{-3}$ K / s and below 10^{-3} K / s in the other sections. Even for the highest power density of 150 MW / m^2, temperature in the central part of the test module is around 100°C, pressure is constant of P = $1.5x10^{-5}$ Pa during the entire injection. In this shot the maximum temperature of the test module is 180°C at the down stream of the test module due to the same reason in section 5.2.6. Measurement of outgassing flux by the build-up method indicates also a steady state outgassing of Q = $3x10^{-7}$ Pa m^3 / s, q = $2x10^{-7}$ Pa m^3 / s m^2.

6 DISCUSSION

6.1 Desorption models

6.1.1 Modeling of surface desorption

5.2.6 Control of the temperature rise rate

Without active cooling, the temperature increases linearly with time. By cooling the test module and the connection waveguides with an air flow rate of 700 N l / min, the temperature rise rate is reduced from 0.3°C / s to 0.025°C / s as shown in Fig. 43 in the case of injection at 50 MW / m^2. This allows, for this power level, to extend the RF injection duration from 32 min to 101 min with initial temperature Ti = 20°C until the maximum temperature reaches 500°C as illustrated in Fig. 44. Air cooling has also an effect on the temperature profile as shown in Fig. 45. Heat exchanges in down stream is not sufficient because of short cooling channel due to lack of space in the vacuum chamber. However an Arrhenius plot log Q vs 1 / T shows a similar temperature dependence of the outgassing with a larger outgassing by a factor of 3 at T = 500°C as shown in Fig. 46. This large outgassing can be explained by a higher temperature of the down stream section of the test module. The outgassing flux Q at 500°C is around $5x10^{-6}$ Pa m^3 / s (q ~ $3x10^{-6}$ Pa m^3 / s m^2).

5.2.7 Stationary outgassing

Long RF injection is performed from room temperature with water cooling of the test module at flow rate of 12.5 l / min. Quasi-stationary temperatures are obtained all along the test module and the connection waveguides up to a power level of 150 MW / m^2 after 30 min of RF power injection as shown in Fig. 47. The largest temperature rise rate at the down stream section is about $5x10^{-3}$ K / s and below 10^{-3} K / s in the other sections. Even for the highest power density of 150 MW / m^2, temperature in the central part of the test module is around 100°C, pressure is constant of P = $1.5x10^{-5}$ Pa during the entire injection. In this shot the maximum temperature of the test module is 180°C at the down stream of the test module due to the same reason in section 5.2.6. Measurement of outgassing flux by the build-up method indicates also a steady state outgassing of Q = $3x10^{-7}$ Pa m^3 / s, q = $2x10^{-7}$ Pa m^3 / s m^2.

6 DISCUSSION

6.1 Desorption models

6.1.1 Modeling of surface desorption

Outgassing can be described from a surface desorption model taking account of surface trapping sites[7]. In this model molecules in the gas phase are in equilibrium with trapped atoms or molecules on the surface. Thermal energy provided by baking competes with the binding energy of the atom or molecule to the surface named as the activation energy E. The rate of molecules leaving from the surface, the desorption rate $q_{des}(t)$, is described by a standard chemical kinetic equation. This outgassing rate $q_{des}(t)$ is proportional to the number of available atoms or molecules σ on the surface and to an exponential term which represents the temperature dependence of the equilibrium :

$$q_{des}(t) = -d\sigma / dt = \nu_n \sigma^n \exp (- E / k T), \qquad (6)$$

where ν_n is a constant, n is the order of the reaction, k Boltzmann constant, and T temperature. For example, in the case of H_2, if the molecule is atomically adsorbed on the surface, the desorption process is expressed as

$$H^{ads} + H^{ads} \text{ (on the surface) } \text{-----> } H_2^{des} \text{ (in the space)} \qquad n = 2 \quad (7)$$

If H_2 is adsorbed in the molecular state, the desorption process is the following :

$$H_2^{ads} \text{ ----> } H_2^{des} \qquad n = 1 \quad (8)$$

This equation can be alytically solved when E and ν_n are presumed independent of σ :

n = 1 case

$$q_{des}(T(t)) = q_0 \exp (-E . (1/T - 1/T_0)) . \exp (-\nu_1 \int_0^t \exp (- E/kT) dt), \quad (9)$$

n = 2 case

$$q_{des}(T(t)) = q_0 \exp (-E . (1/T - 1/T_0)) . (1 + (q_0 \nu_2)^{0.5} \exp (E / 2kT_0) \int_0^t \exp (- E / kT) dt)^2, \quad (10)$$

where q_0 is initial outgassing rate given by $q_0 = - d\sigma / dt$ at initial temperature $T_0 = T (t=0)$.

As an example, $q (T(t))$ is computed for a off-set linear increase in the temperature $T (t) = T_0 + b t$ with $T_0 = 200°C$, $q_0 = 1.33 \times 10^{-6}$ Pa m^3 / s m^2 , b = 0.32

K / s and E = 0.85 eV in the case of a second order reaction as shown in Fig. 48. Computation has been in for three cases of initial coverage σ_0 = 0.47, 1.4 and 4.7x10^{15} molecules / cm^2 which roughly correspond to respectively 1, 3 and 10 monolayers on the surface. Tm is defined as the temperature of the maximum outgassing. When temperature T is less than ninety percents of Tm, the second exponential term in eq. (9) and (10) is close to 1 and can be neglected. Therefore, a semi-log plot of q vs 1 / T gives a line of slope -E for both cases of desorption. During this temperature range, the surface molecules coverage σ is quasi constant as shown in the lower side of Fig. 48.

Effect of RF power is also investigated by varying the temperature increase rate b = dT / dt which is proportional to the power in the case of no cooling. Figure 49 shows that the initial slope, proportional to -E, is not affected. This is consistent with the experimental results in figure 34. The only effect predicted by this model occurs when the temperature T is closed to Tm, the larger b leads the higher Tm and the larger outgassing rate.

6.1.2 Modeling of diffusion from the bulk

At higher temperature, diffusion from the bulk may become significant. Diffusion process is expressed by the second order differential equation $\frac{\partial c}{\partial t} = D \bullet \frac{\partial^2 c}{\partial x^2}$:

$$\frac{\partial c}{\partial t} = D \bullet \frac{\partial^2 c}{\partial x^2}, \tag{11}$$

where c (x, t) is the density of molecules / atoms in the bulk and D the diffusion coefficient in the bulk. The D has the following temperature dependence :

$$D(T) = D_0 \exp(-E_{dif} / k T), \tag{12}$$

where D_0 is constant and E_{dif} is activation energy for a diffusion process. Outgassing rate Q_{dif} due to a diffusion process from a plate is given by :

$$q_{dif} = -D \frac{\partial c}{\partial x} \quad (\text{at edge} : x = 0). \tag{13}$$

If $D(T) \cdot t / d^2 > 0.025$ (d : thickness of the plate), then the density distribution function becomes in one dimensional case as follows :

$$c(x, t) = c_0 (4 / \pi) \sin(\pi x / d) \exp(-\pi^2 D(T) t / d^2), \tag{14}$$

where c_0 is the initial density and constant across the plane. After baking at a temperature of T_b during a period of t_b, the density c (x, t) approximately becomes at a temperature T :

$$c(x,t) = c_0 (4/\pi) \sin(\pi x/d) \exp(-\pi^2 D(T_b) t_b / d^2) \exp(-\pi^2 D(T) t / d^2). \quad (15)$$

When T is lower than T_b, D (T) is usually small and the second exponential factor becomes unity. The outgassing rate will be :

$$q(t) = (4 c_0 D(T(t))/d) \exp(-\pi^2 D(T_b) t_b / d^2), \quad (16)$$
$$= (4 c_0 D_0 / d) \exp(-\pi^2 D(T_b) t_b / d^2) \exp(-E_{dif} / k T(t)). \quad (17)$$

Equation (17) has the same temperature dependence of surface desorption when the integral term in eq. (9) and (10) is negligible. The first exponential term in eq. (17) may express the baking effect at high temperature, namely it means reducing rate of residual gas in the plate as illustrated in figure 50. For instance, outgassing rate and baking effect are shown in Fig. 51 for the case of H_2 in stainless steel with the following parameters :

$D_0 = 1.658 \times 10^{-6}$ m^2 / sec
$E_{dif} = 0.8$ eV
$c_0 = 4 \times 10^3$ Pa m^3 / m^3
$d = 2 \times 10^{-3}$ m.

For H_2, it is indeed possible to pump out interstitial gas from a 2 mm thick plate. After 450°C - 60 hours baking , gas concentration of H_2 is reduced by a factor of 10 as illustrated in Fig. 51. If the activation energy E_{dif} is slightly lower, the reduction is even more drastic, a 100-fold reduction is obtained for E_{dif} = 0.65 eV. This calculation suggests that the baking at high temperature (T > 450°C) is critical to reduce outgassing rate as far as hydrogen diffusion from the bulk is concerned.

Diffusion of H_2 in copper has been studied by many authors[8, 9, 10]. The activation energy for the diffusion coefficient is found to be smaller than for stainless Steel : E_{dif} = 0.3 - 0.4 eV, with a pre-exponential factor D_0 in the range of 0.2 - 1.1×10^{-6} m^2 / s, leading to a diffusion coefficient of 1 - 2×10^{-9} m^2 / s at 450°C. Baking at high temperature should be even more efficient than for stainless steel with lower D = 10^{-10} m^2 / s at 450°C. For other gases, very little has been published. The diffusion coefficients are much smaller, the diffusion coefficient D for helium is only 2×10^{-13} m^2 / s at T = 450°C [10] and for bigger molecules such as H_2O, CO, CO_2, the diffusion process is

even smaller. For such molecules, diffusion process may be responsible for outgassing coming from a thin layer, close to the surface, of typical thickness δ given by the relation:

$$D(T)\,t / \delta^2 \sim 1. \qquad (18)$$

Waveguides are heated between 400 and 500°C for a typical duration of the order of 100 s in the outgassing experiments. Eq.(18) leads to an effective desorption from the bulk on a thickness $\delta = 5 \times 10^{-6}$ m (~ 10^4 monolayers). This could explain the transition in outgassing observed at T ~ 400°C from a surface limited desorption to a bulk limited desorption with a higher activation energy.

6.1.3 Modeling of adsorption

When the surface molecule coverage is very low (σ < 1 monolayer), the adsorption process becomes very important. According to gas kinetic theory, a flux of colliding molecules on a unit surface per unit time is given by :

$$\phi = k\,P\,(T / M)^{0.5}, \qquad (19)$$

where P is gas pressure, T temperature, k Boltzmann constant and M mass of molecule. A fraction s of these colliding molecules will be stuck on the surface. The sticking coefficient s depends on the surface coverage, the chemical affinity of the molecule and the surface metal. This adsorption process ca be characterized by a pumping speed S_{ads} of the surface :

$$S_{ads} = s\,\phi / P = k\,(T / M)^{0.5}\,s. \qquad (20)$$

For molecules with a high chemical affinity such as H_2O or CO_2 on a surface with a low molecule coverage σ, then s ~ 1 and the pumping speed S_{ads} is large : 150 m^3 / s m^2 for H_2O at T = 20°C. This pumping speed is very large compared with that of a usual additional pumping unit and a low molecules coverage is never obtained. When the surface pumping becomes efficient, desorbed molecules are re-adsorbed. Consequently, the decrease in outgassing rate, as predicted by a simple desorption model as shown in Fig. 48, is never observed. The re-adsorption process is even more clear in the case of the longest shot of 101-min injection where the decrease of outgassing is expected after 30 min of injection in taking into account of baking effect due to diffusion process.

6.2 Evaluation of the activation energy

It has been shown in Fig. 34 that the activation energy deduced from Log Q vs 1 / T curve has near values for the main species. Therefore a " global " activation energy can be defined from the total pressure measurement. Due to the low outgassing rate, accuracy is rather poor and error bar is estimated to be +/- 0.2 eV. For the shots within insufficient conditioning phase, activation energy of 0.9 eV (20 kcal / mole) is measured. This value is close to the one obtained in the previous experiments[11]. Much lower values of E_d are obtained around 0.3 eV after shot number #97 as shown in Fig. 52, E_d shows a large scattering. Average value is 0.27 eV with standard deviation of 0.19 eV. This value is confirmed by measurement of the outgassing rate with the build up method as shown in Fig. 53 which indicates an average E_d of 0.34 eV with a standard deviation of 0.15 eV.

7. CONCLUSIONS

It is very important to measure outgassing rate from waveguides of LHCD antenna during steady state RF injection. Therefore the outgassing characteristics are investigated by using a four divided waveguides named as the test module. The test module is made of dispersion strengthened copper, and is fabricated using the diffusion bonding method. The test module shows good RF properties : low VSWR and low RF losses consistent with calculations. However the increase in power reflection during long pulses suggests some elastic deformation of the module. Moreover, at high power level, a resonance phenomena occurred above 450°C. It is interpreted from calculation as a consequence of a slight unbalance in the height of the four sub-waveguides of the test module. The test module shows high power capability up to 200 MW / m^2.

Outgassing flux and related outgassing rate of the module has been measured in various experimental conditions such as initial temperature, RF power, different cooling, some thermal treatments. Averaged on the whole surface of the test module, the outgassing rate measured at 400°C decreases as a result of conditioning from 5×10^{-4} to 1×10^{-6} Pa m^3 / s m^2. The lower outgassing rate below 10^{-5} Pa m^3 / s m^2 is already obtained before the thermal treatment of baking at 450°C for 10 hours. The reduction in outgassing rate due to strong conditioning effect is brought by the high temperature baking during the RF injection. Namely the test module is actually baked between 400 and 500°C during accumulated time of about 3 hours by injecting 6 GJ of RF power. These characteristics of outgassing are consistent with previous results obtained :

6.2 Evaluation of the activation energy

It has been shown in Fig. 34 that the activation energy deduced from Log Q vs 1 / T curve has near values for the main species. Therefore a " global " activation energy can be defined from the total pressure measurement. Due to the low outgassing rate, accuracy is rather poor and error bar is estimated to be +/- 0.2 eV. For the shots within insufficient conditioning phase, activation energy of 0.9 eV (20 kcal / mole) is measured. This value is close to the one obtained in the previous experiments[11]. Much lower values of E_d are obtained around 0.3 eV after shot number #97 as shown in Fig. 52, E_d shows a large scattering. Average value is 0.27 eV with standard deviation of 0.19 eV. This value is confirmed by measurement of the outgassing rate with the build up method as shown in Fig. 53 which indicates an average E_d of 0.34 eV with a standard deviation of 0.15 eV.

7. CONCLUSIONS

It is very important to measure outgassing rate from waveguides of LHCD antenna during steady state RF injection. Therefore the outgassing characteristics are investigated by using a four divided waveguides named as the test module. The test module is made of dispersion strengthened copper, and is fabricated using the diffusion bonding method. The test module shows good RF properties : low VSWR and low RF losses consistent with calculations. However the increase in power reflection during long pulses suggests some elastic deformation of the module. Moreover, at high power level, a resonance phenomena occurred above 450°C. It is interpreted from calculation as a consequence of a slight unbalance in the height of the four sub-waveguides of the test module. The test module shows high power capability up to 200 MW / m^2.

Outgassing flux and related outgassing rate of the module has been measured in various experimental conditions such as initial temperature, RF power, different cooling, some thermal treatments. Averaged on the whole surface of the test module, the outgassing rate measured at 400°C decreases as a result of conditioning from 5×10^{-4} to 1×10^{-6} Pa m^3 / s m^2. The lower outgassing rate below 10^{-5} Pa m^3 / s m^2 is already obtained before the thermal treatment of baking at 450°C for 10 hours. The reduction in outgassing rate due to strong conditioning effect is brought by the high temperature baking during the RF injection. Namely the test module is actually baked between 400 and 500°C during accumulated time of about 3 hours by injecting 6 GJ of RF power. These characteristics of outgassing are consistent with previous results obtained :

-- from the Tore Supra and JET prototype module with low temperature baking of 300°C and small conditioning effect due to a low temperature baking above 350°C by the RF injection less than 10 min,
-- from TdeV prototype module with high temperature baking of 450°C.

Outgassing model of desorption shows that a semi-log plot as outgassing Q vs inverse temperature 1 / T should follow a straight line over a wide range of temperature. This tendency is indeed observed in most cases and the RF induced baking is not different from standard methods of baking. In particular, outgassing rate is independent of injected RF power. Saturation in the outgassing is never observed, whereas calculation indicates that such a saturation should occur at a temperature between 350 and 450°C. The temperature is depending upon the initial molecules coverage on a surface and is controlled by air cooling. The difference between calculation and measurements means that re-adsorption at the surface does occur and coverage in molecules can not be reduced by more than 50 % of the initial value. This is confirmed by deuterium injection before / during RF injection which shows no further release of deuterium and no pumping effect of the walls of the waveguides indicating a still high molecules coverage.

Rate of gas composition is quasi constant up to 400°C, H_2O and CO_2 gases mainly come from the test module. In higher temperature above 400°C, CO_2 and CO concentrations increase. H_2 content is found small as 20 %, whereas H_2 is usually main residual gas in iron-based material vacuum chamber. H_2 gas suddenly increases up to 60 % when a breakdown occurs. After baking at 450°C in D_2 pressure of 10 Pa, main D atoms of the desorbed gases exist in water molecules.

Global activation energy E_d in early conditioning phase is ~ 0.9 eV, but then decreases to 0.3 eV. This decrease may be due to the change in coverage molecules from 10 monolayers to few monolayers. The further increase in the outgassing at higher temperature above 400°C could be explained by a diffusion process from a thin layer ($\sim 5 \times 10^{-6}$ m) close to the surface, strongly enhanced for CO, CO_2, and H_2O.

For the pumping of large CW antennae, the following design values of outgassing rate can be given :

After 300°C baking $q = 10^{-5}$ Pa m^3 / s m^2 at 300°C
10^{-4} Pa m^3 / s m^2 at 400°C

After 450°C baking $q = 2 \times 10^{-7}$ Pa m^3 / s m^2 at 300°C

10^{-6} Pa m^3 / s m^2 at 400°C.

These outgassing rates are low enough to require a reasonable pumping speed for an LHCD antenna of several tens of MW. Moreover stationary temperature and outgassing are obtained by water cooling under 150 MW / m^2 RF transmission, temperature is around 120°C and outgassing rate is low level of 10^{-7} Pa m^3 / s m^2. This leads a steady state LHCD antenna.

ACKNOWLEDGMENTS

This work has performed under the Agreement between The Japan Atomic Energy Research Institute (JAERI) and The Commissariat a l'Energie Atomique (CEA) on cooperative activities concerning a lower hybrid antenna module.

The authors would like to express their thanks to all members of the RF Facility Division and RF Heating Laboratory of JAERI, and LHRF group of CEA Cadarache for their continuous support.

10^{-6} Pa m^3 / s m^2 at 400°C.

These outgassing rates are low enough to require a reasonable pumping speed for an LHCD antenna of several tens of MW. Moreover stationary temperature and outgassing are obtained by water cooling under 150 MW / m^2 RF transmission, temperature is around 120°C and outgassing rate is low level of 10^{-7} Pa m^3 / s m^2. This leads a steady state LHCD antenna.

ACKNOWLEDGMENTS

This work has performed under the Agreement between The Japan Atomic Energy Research Institute (JAERI) and The Commissariat a l'Energie Atomique (CEA) on cooperative activities concerning a lower hybrid antenna module.

The authors would like to express their thanks to all members of the RF Facility Division and RF Heating Laboratory of JAERI, and LHRF group of CEA Cadarache for their continuous support.

REFERENCES

1) G. Rey, R. Aymar, G. Berger-By, Ph. Bibet, P. Hertout, R. Magne, C. Portafaix, G. Tonon : Proc. 15th Symp. on Fusion Technol., p514 (1988).

2) H. Brinkschulte, G. Rey, M. Brusati, A. Ekedahl, C. Gormezano, A. Kaye, M. Lennholm, M. Pain, H. Panissie, J. Plancoulaine : Proc. 16th Symp. on Fusion Technol., p1166 (1990).

3) Y. Demers, J. Bagdoo, P. Brooker, G. A. Chaudron, R. Decoste, A. Dube, V. Fuchs, P. Garcia, R. Gold, V. Glaude, J. M. Guay, F. Guerdain, A. Hubbard, Ph. Jacquet, D. Larose, R. Magne, R. Mireault, G. Rey, A. Robert, I. P. Shkarofsky, M. Shoucri, J. F. Theriault, C. Trudel, L. Vachon : Europhysics Top. Conf. Bruxelles p73 (1992).

4) V. V. Parail, N. Fujisawa, H. Hopman, H. Kimura, W. B. Lindquist, W. M. Nevins, L. Rebuffi, M. Sironi, D. W. Swain, J. G. Wegrove : ITER doc. series, IAEA, Vienna, N° 32 p74 (1991).

5) Y. Ikeda, M. Seki, S. Maebara, K. Wakabayashi, S. Asai, A. Ozaki : Fusion Eng. Design, 23 p33 (1993).

6) M. Goniche, G. Berger-By, P. Bibet, P. Bonnel, C. Gil, J. L. Bruneau, J. J. Capitain, C. C. Klepper, P. Hertout, R. Magne, G. Rey, L. Rodriguez, M. Talvard, G. Tonon : Repport EUR-CEA-PC-1384 (1989).

7) P. A. Redhead : Vacuum 12, p203 (1962).

8) D. N. deWulf, A. J. Bard : J. Electr. Soc., Vol. 132, N° 12 p2965 (1985).

9) T. Tanabe, Y. Yamanishi, K. Sawada, S. Imoto : J. Nucl. Mat. 122-123, p1568 (1984).

10) L. Katz, M. Guinan, R. J. Bary : Phys. Rev. B4, p330 (1971).

11) M. Goniche, Y. Demers, G. Rey, M. Seki, G. Tonon : Le Vide - Les couches minces, vol.48, 264 p411 (1992).

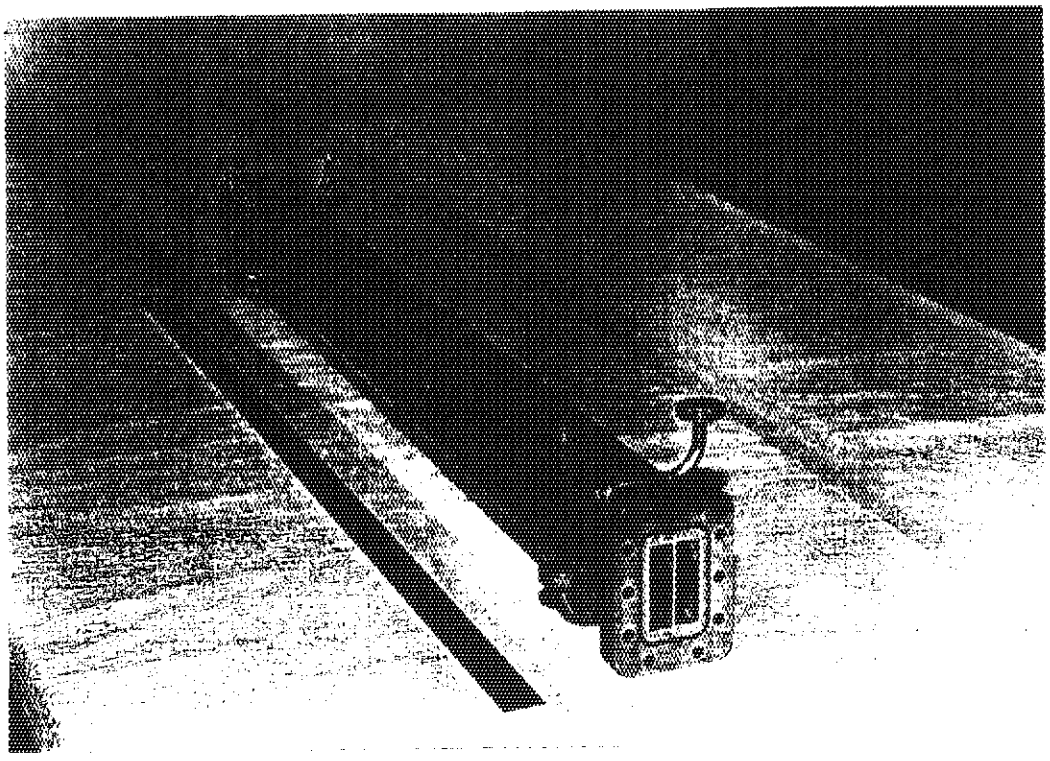

Fig. 1 Photograph of the test module.

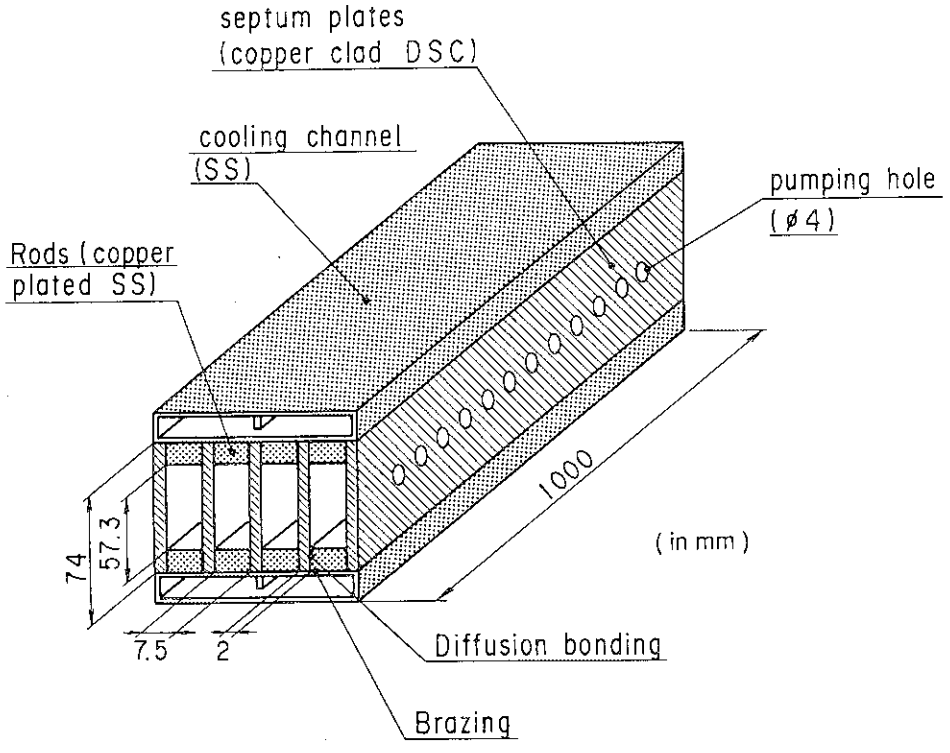

Fig. 2 Schematic drawing of the test module.

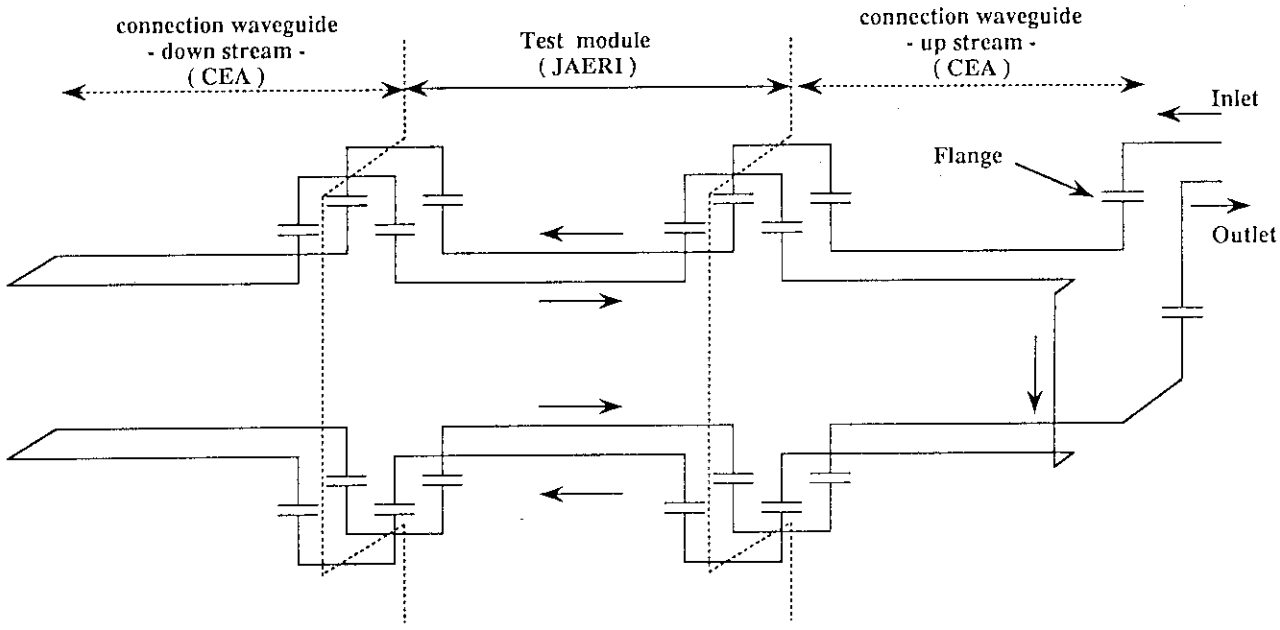

Fig. 3 The cooling channel route.

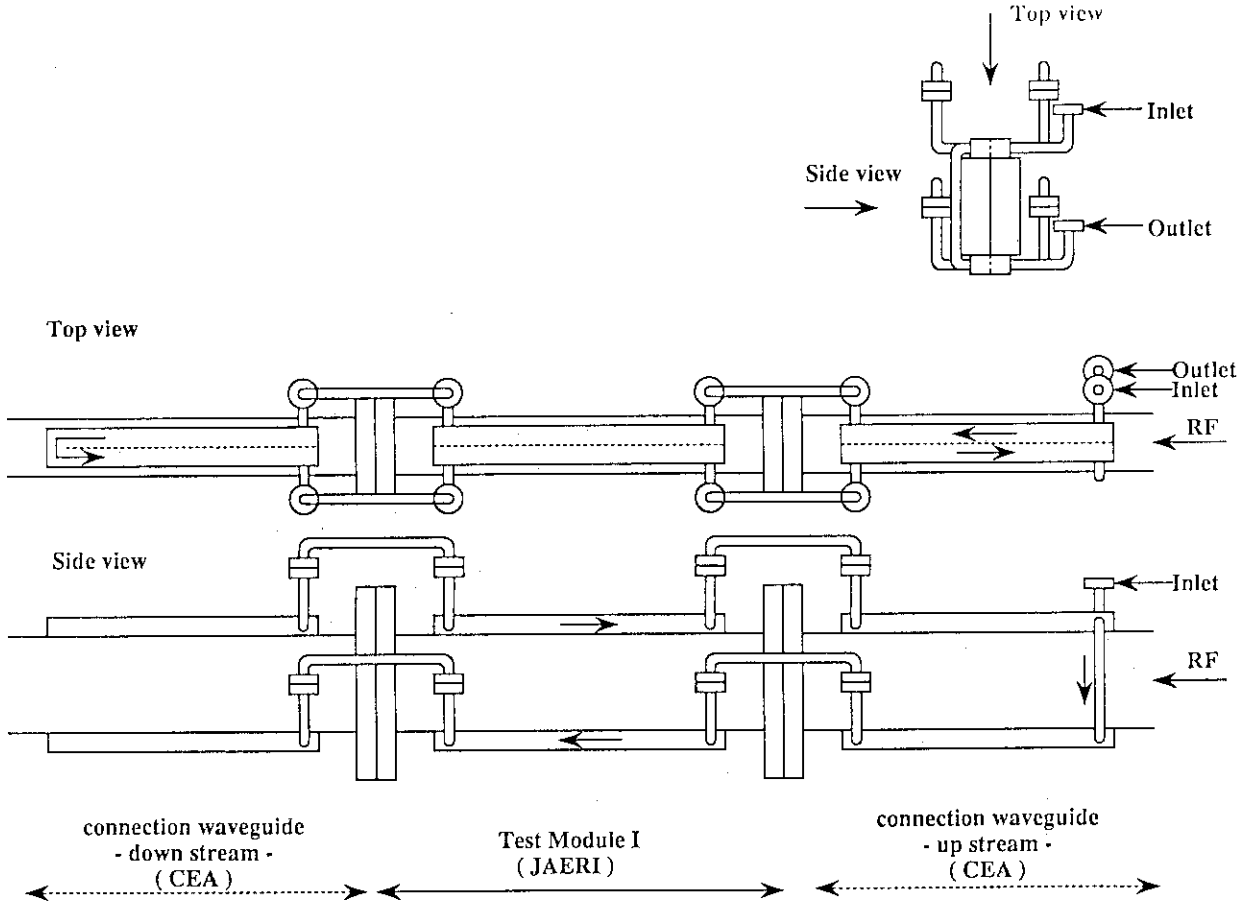

Fig. 4 Schematic drawing of cooling assembling.

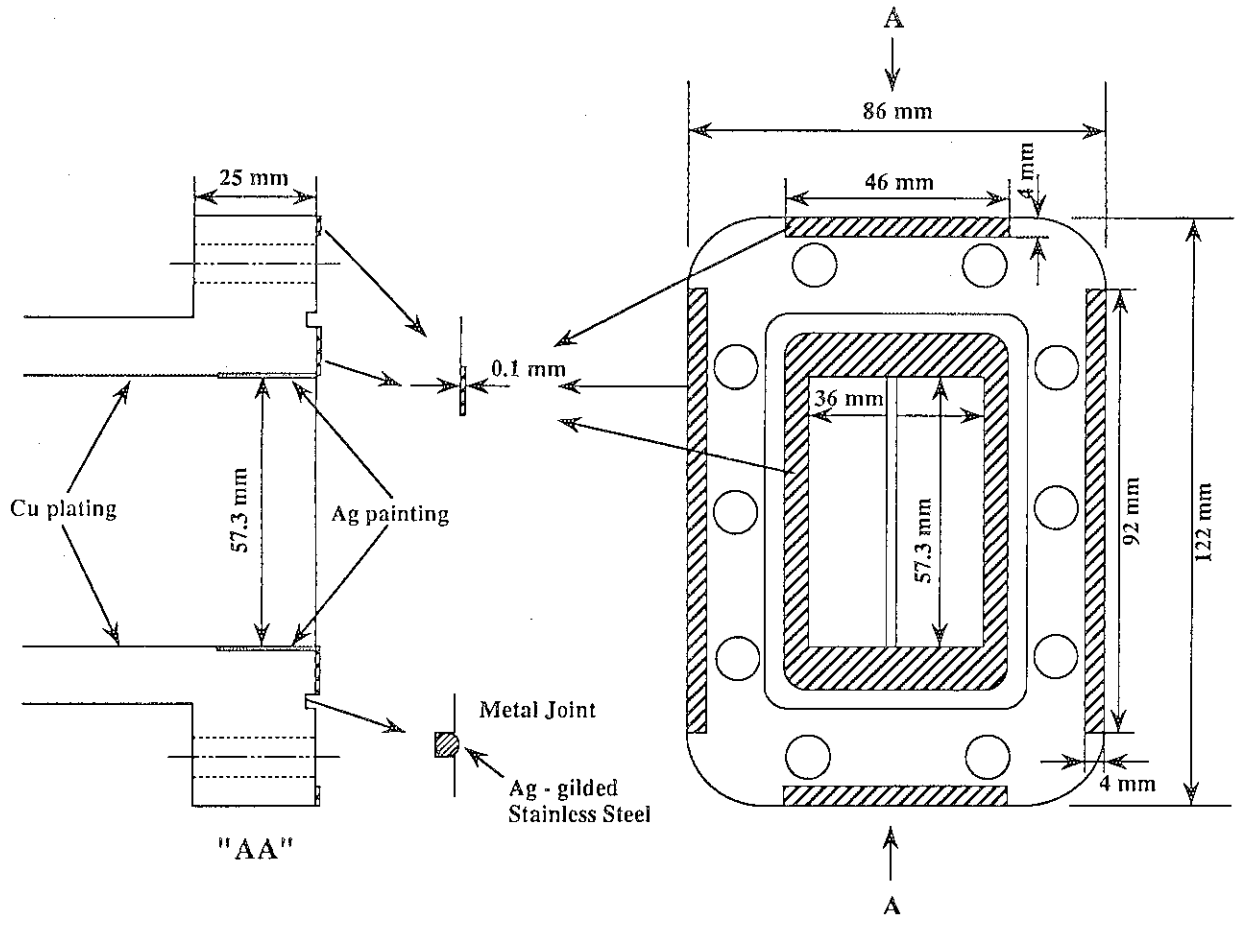

Fig. 5 Schematic drawing of the JAERI flange.

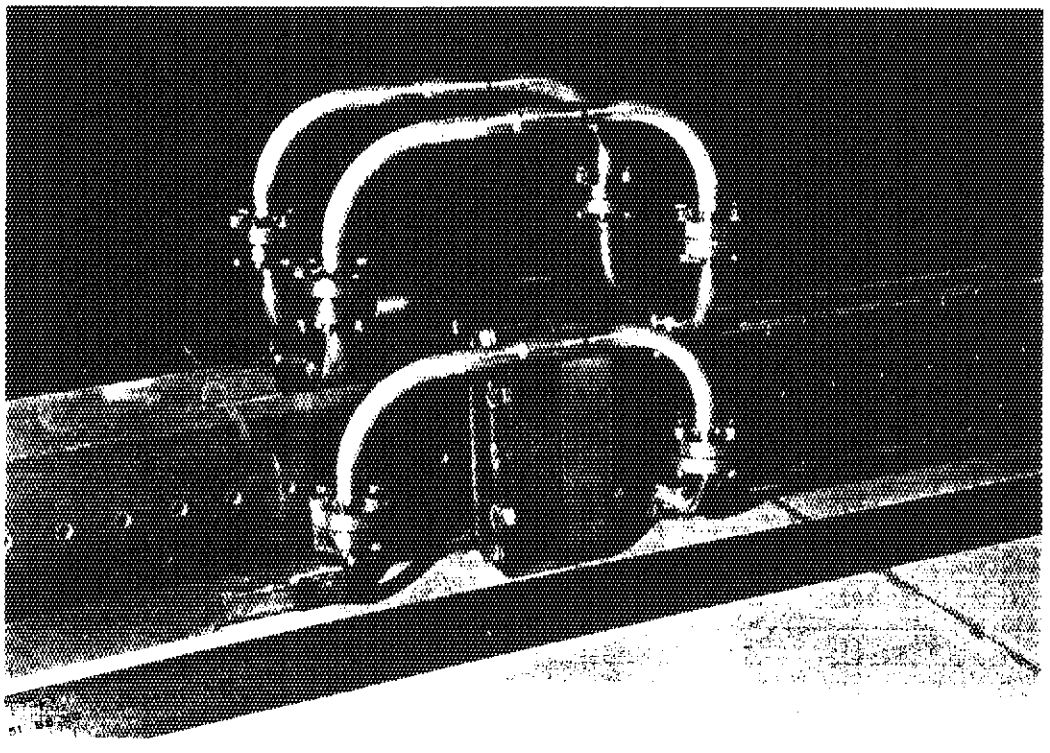

Fig. 6 Photograph of the assembling of the test module to a connection waveguide.

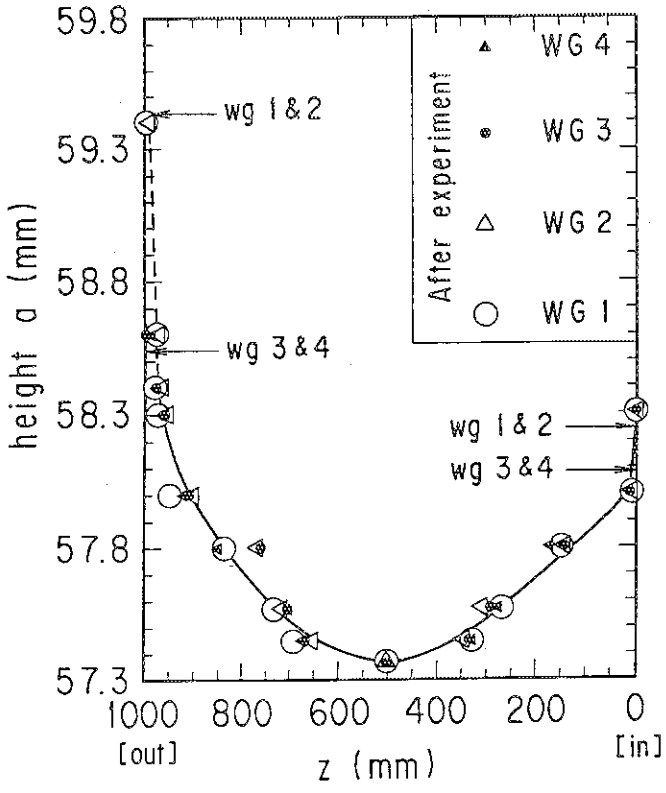

Fig. 7 Measurements of the four waveguides height profile aj (z). Arrows indicate measurements before experiment.

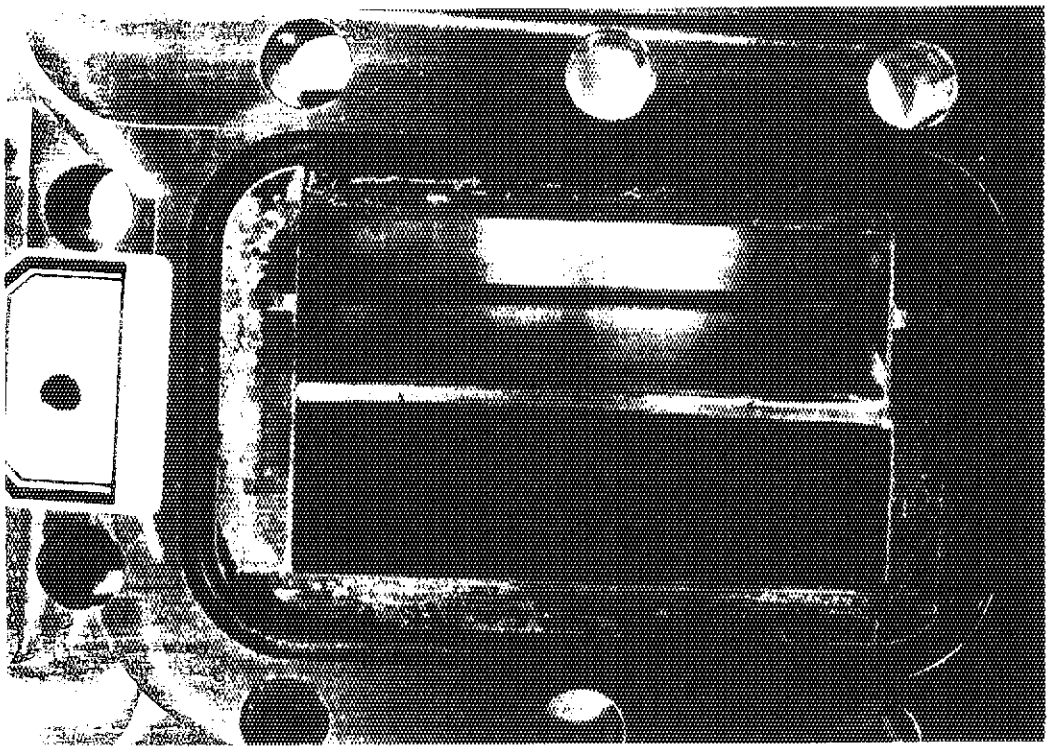

Fig. 8 Photograph showing the down stream flange after experiment.

Fig. 9 Photograph of the experimental set-up.

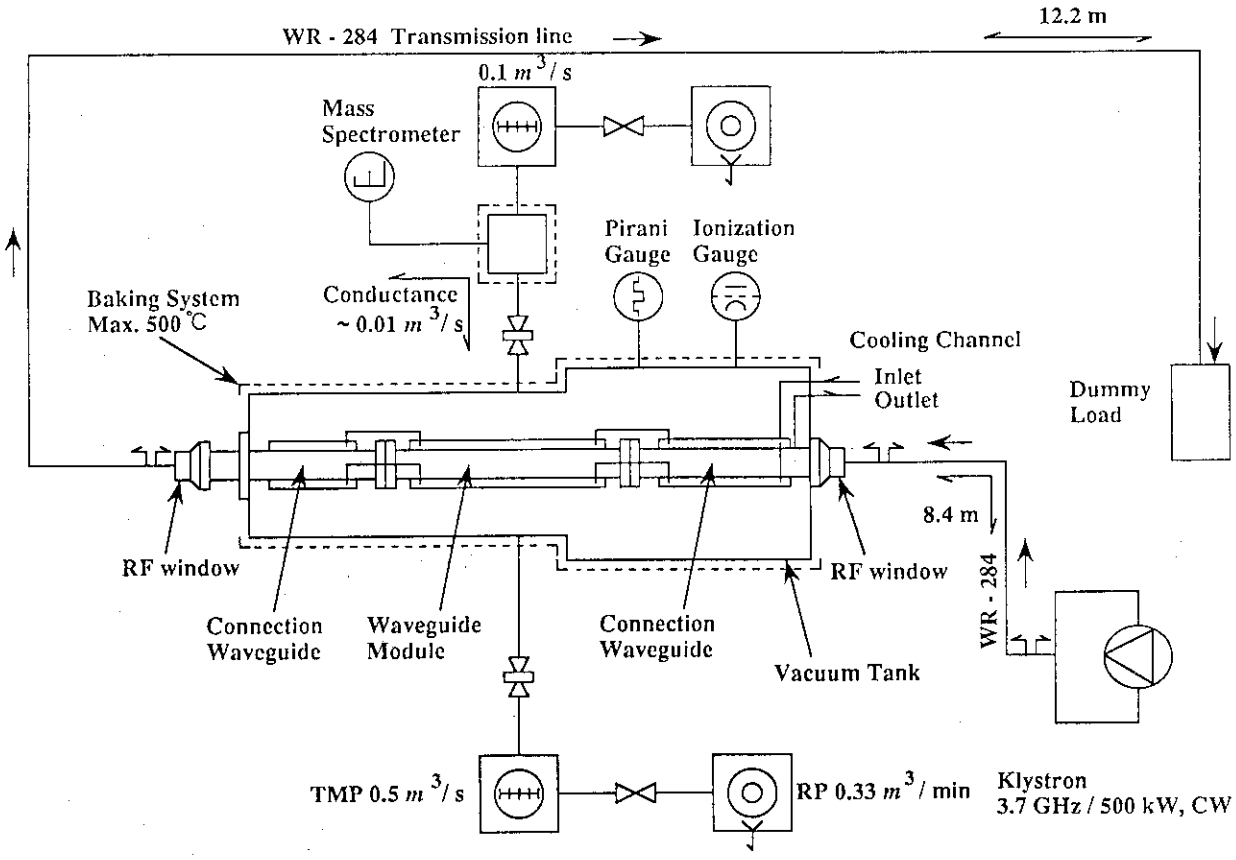

Fig. 10 Sketch of the experimental set-up.

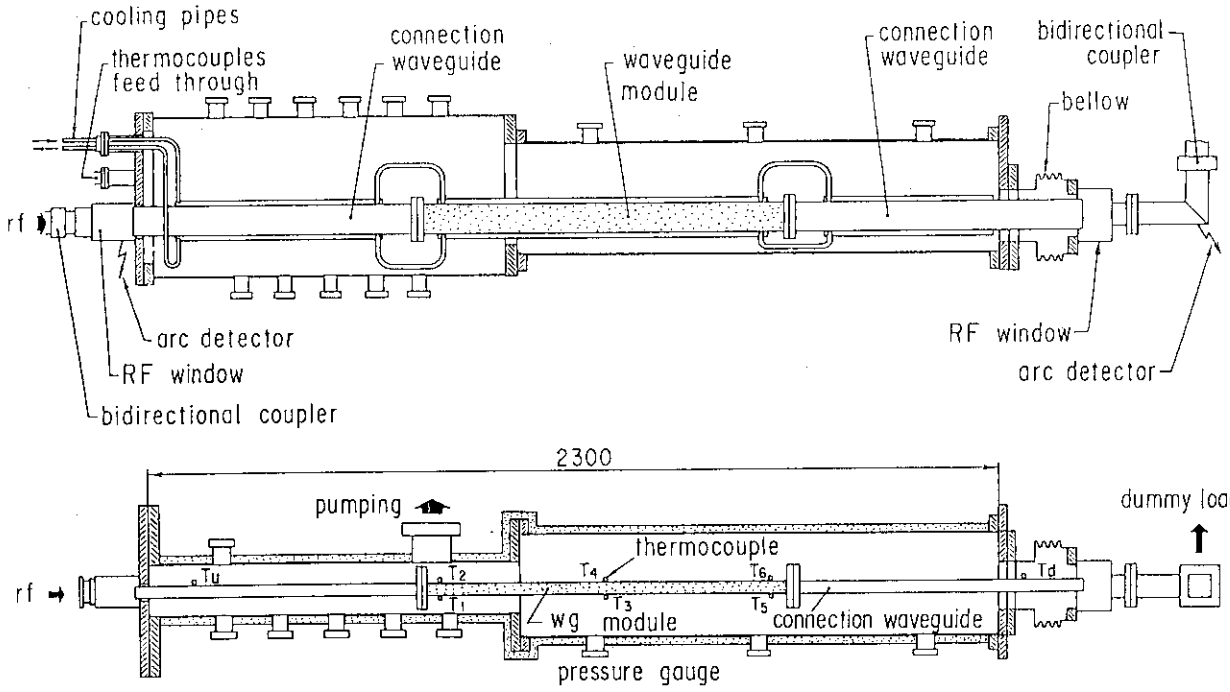

Fig. 11 Drawing of the test module installed in the vacuum tank.

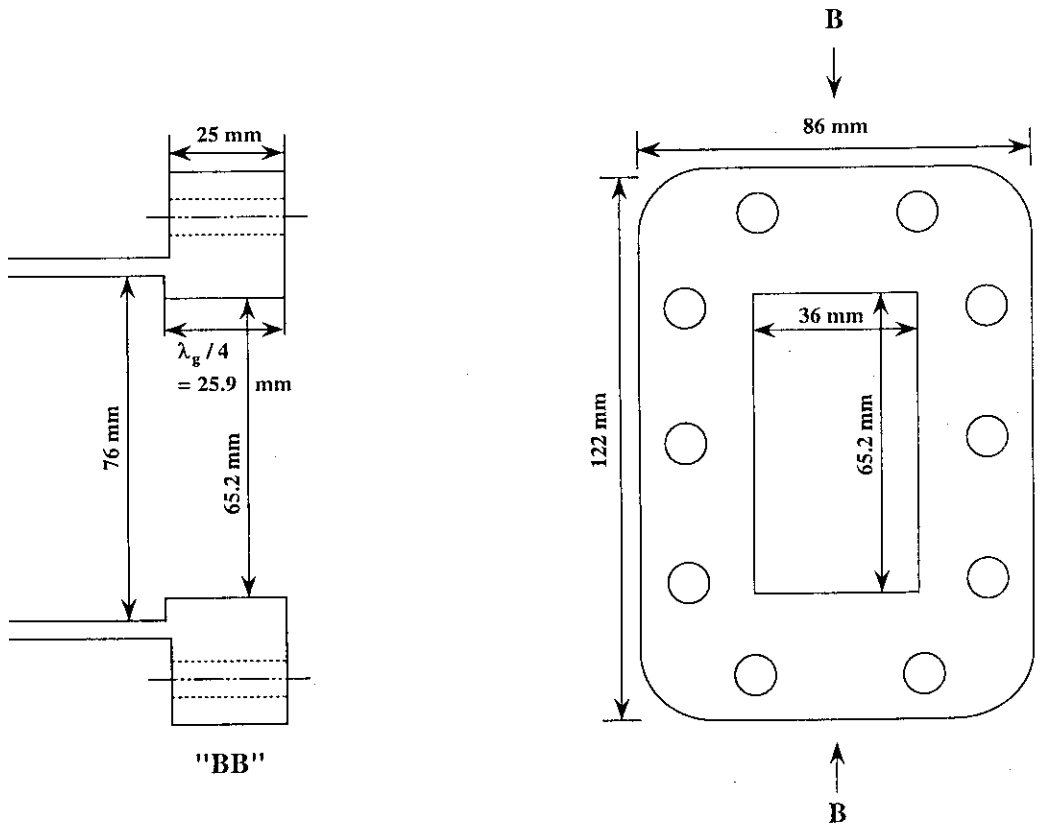

Fig. 12 Schematic drawing of a CEA connection waveguide flange.

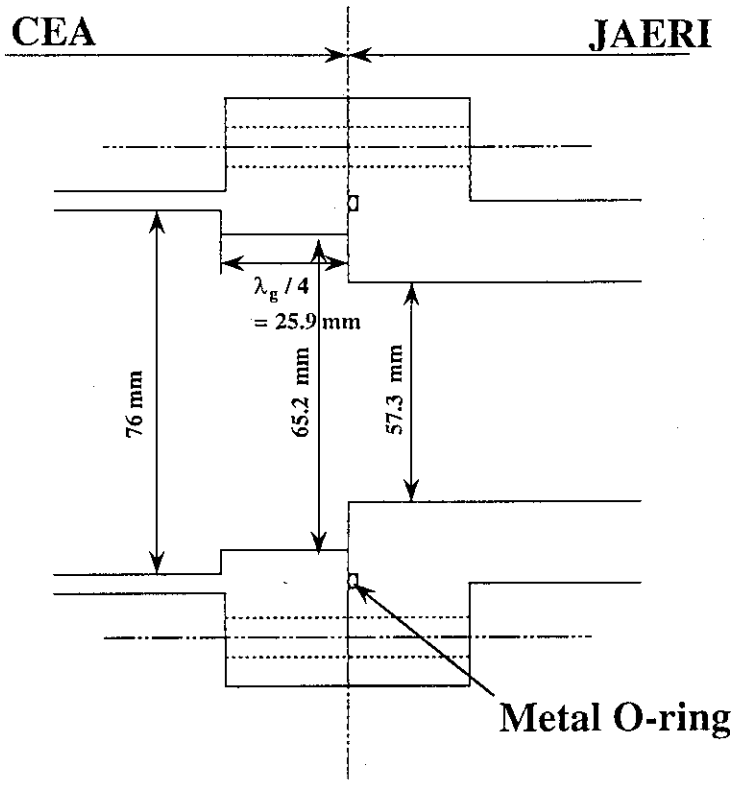

Fig. 13 Schematic drawing of the connected flanges showing the step transformer.

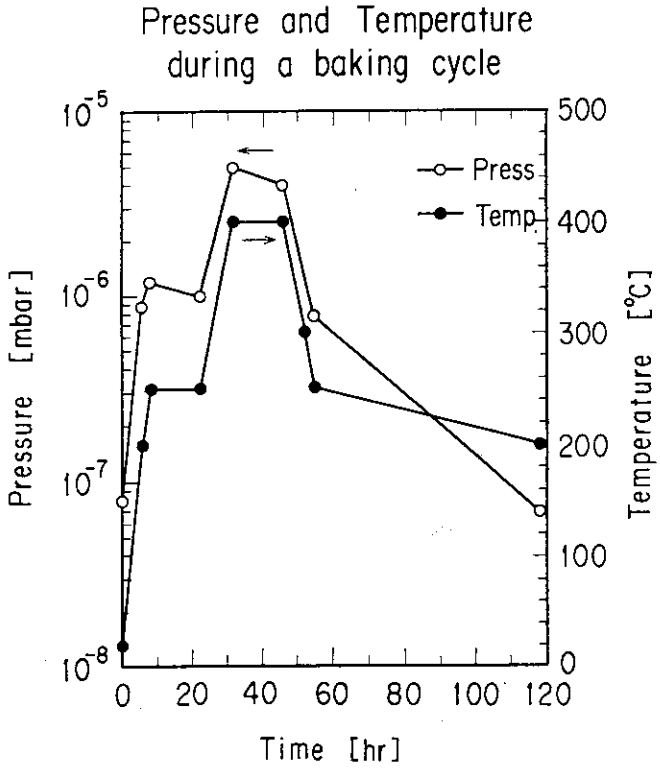

Fig. 14 Temperature and pressure during a baking cycle.

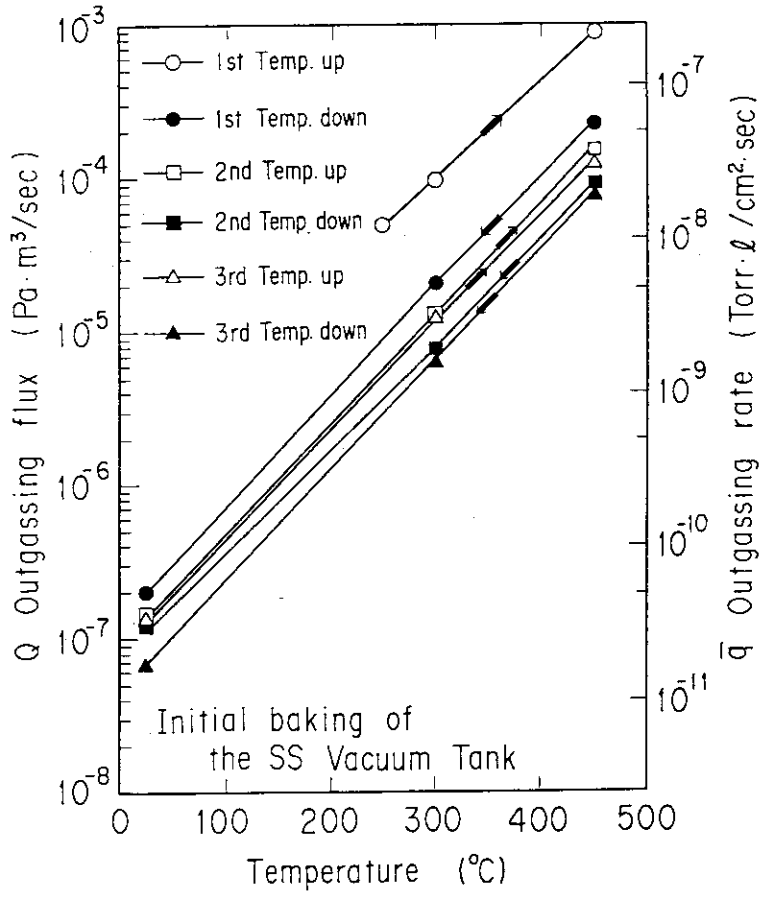

Fig. 15 Initial baking of the stainless steel vacuum tank.

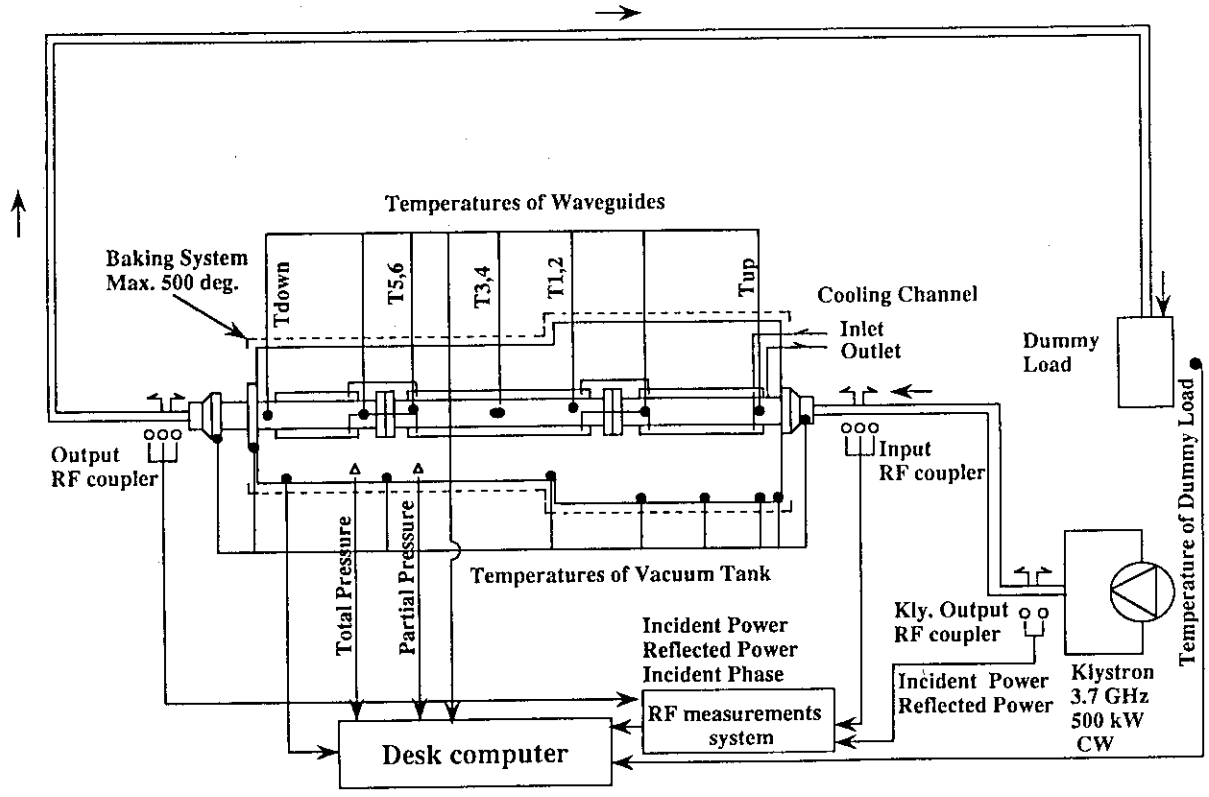

Fig. 16 The measurements system.

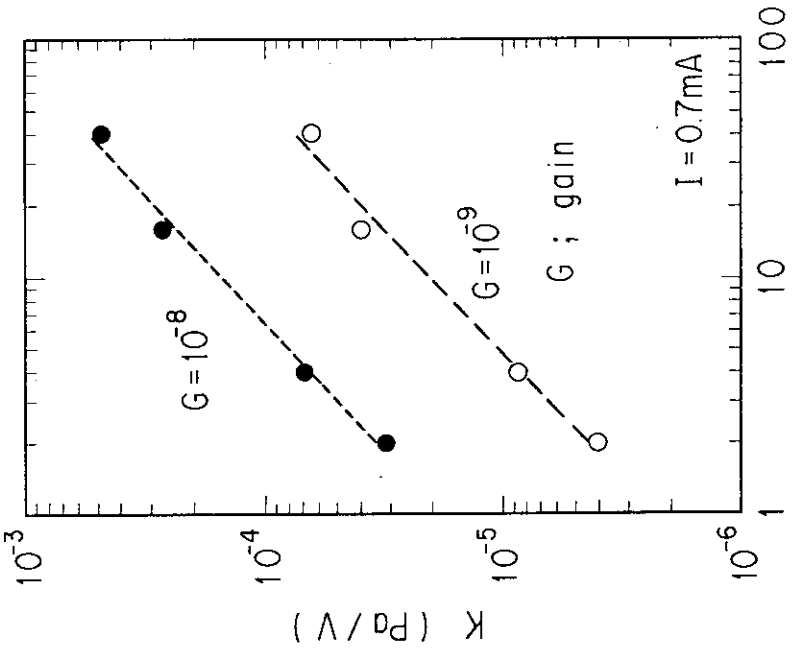

Fig. 18 Calibration of the QMGI12 mass spectrometer.

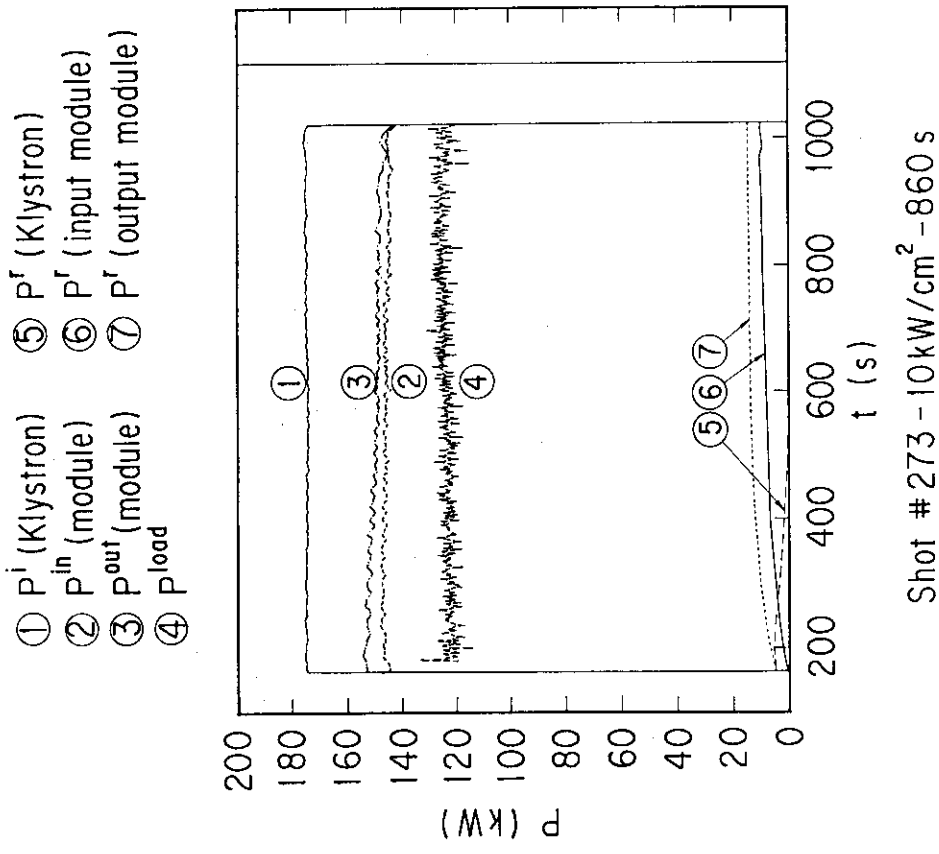

Fig. 17 RF signals shape during a 100 MW/m²-860 s shot.
P_{load} is calculated from calorimetric measurements.

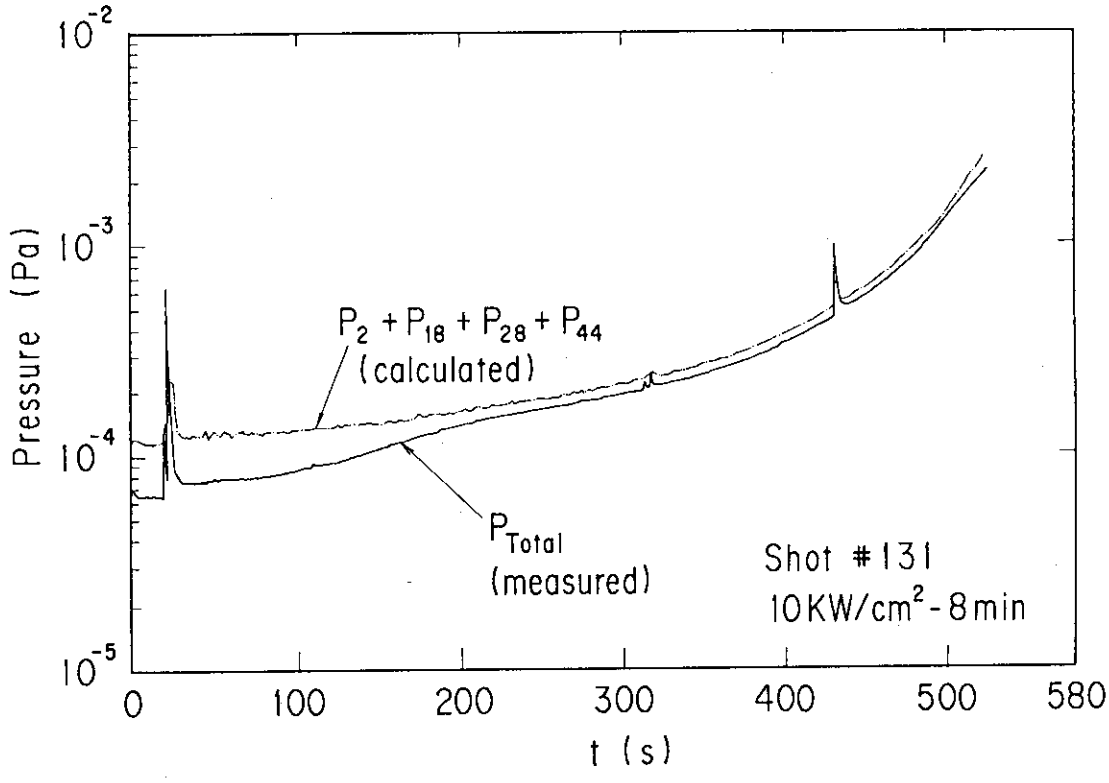

Fig. 19 Comparison of P_{tot} and $P_2 + P_{18} + P_{28} + P_{44}$ during a shot.

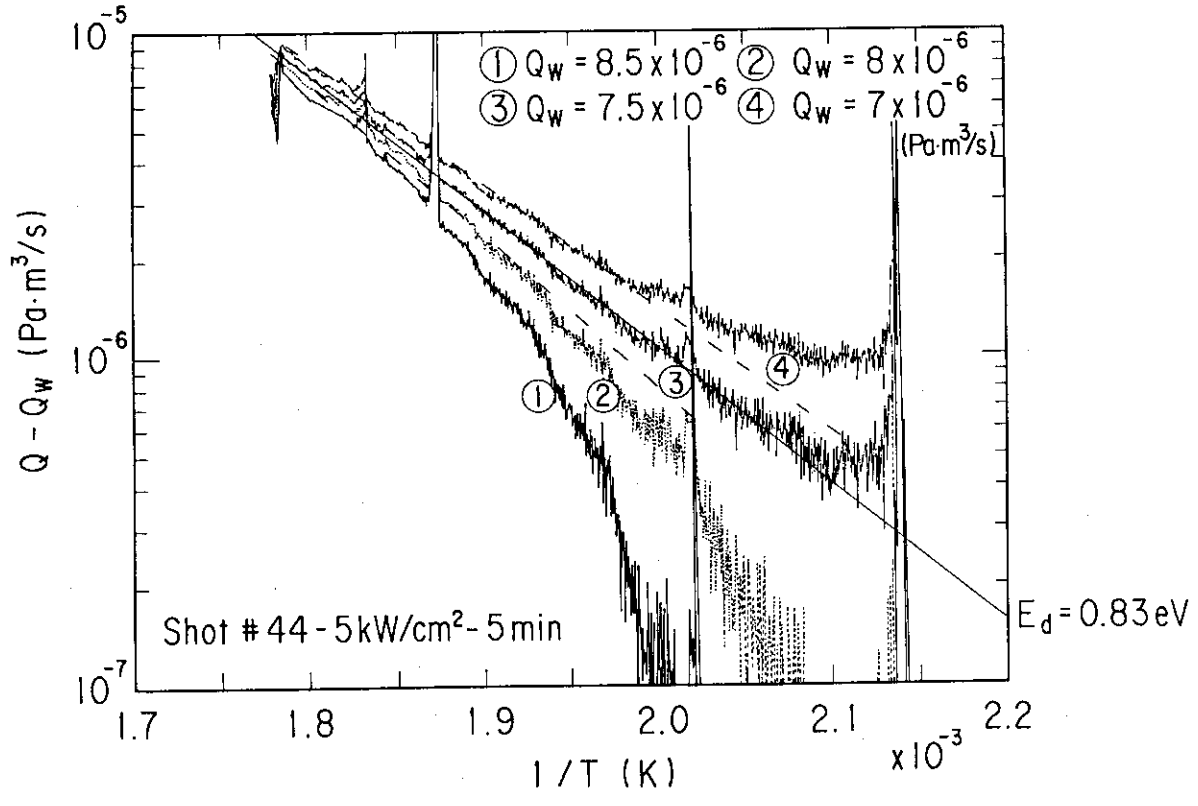

Fig. 20 Q-Qw versus 1/T for different Qw values.

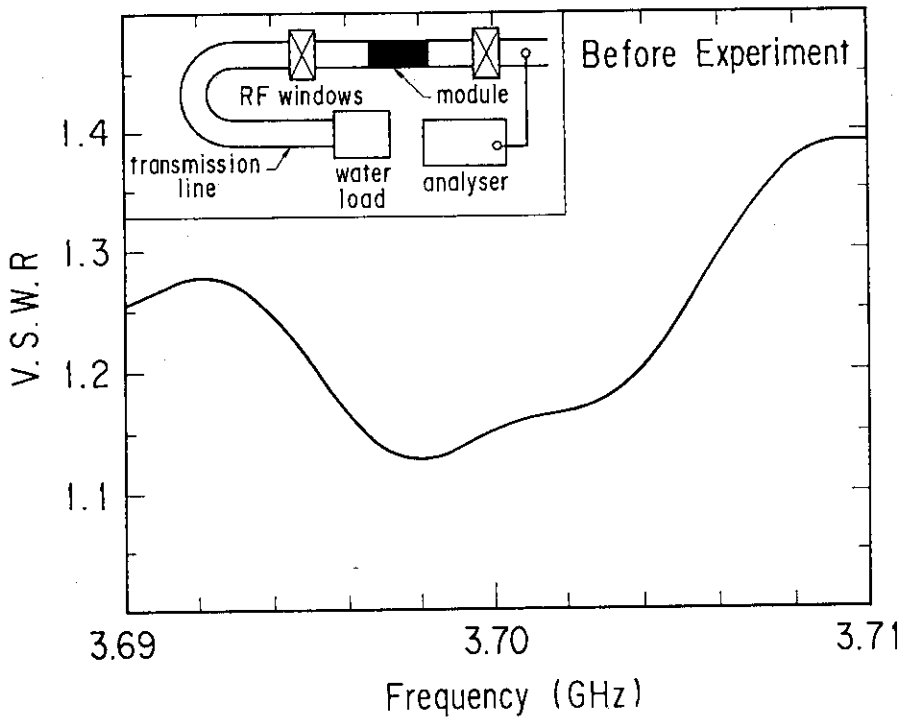

Fig. 21 VSWR of the test module in the 3.69-3.71 GHz band before experiment.

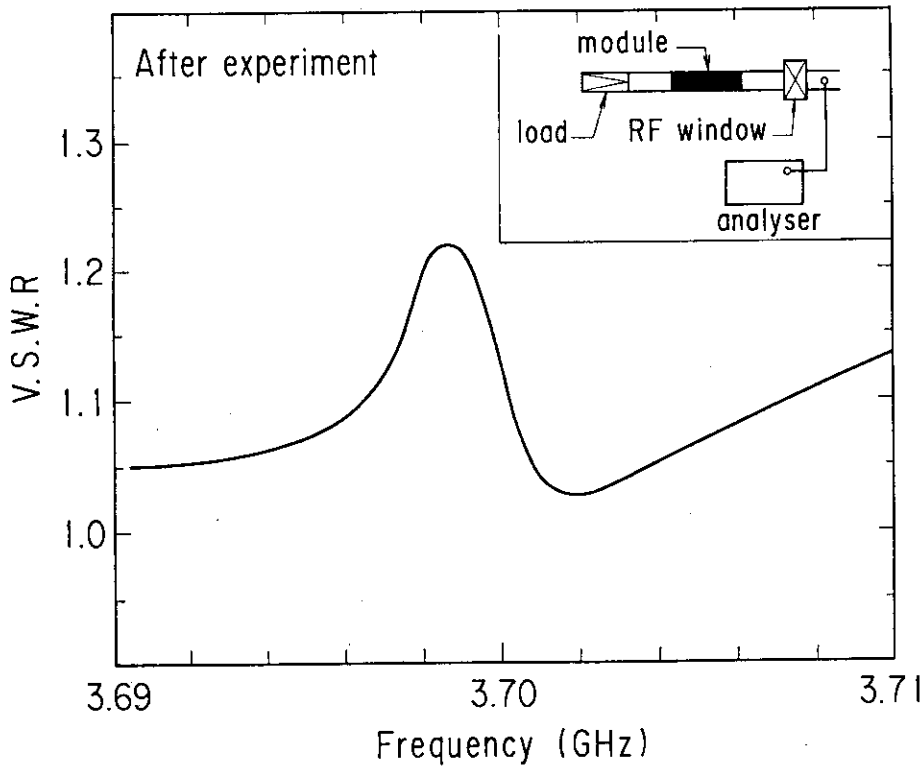

Fig. 22 VSWR of the test module in the 3.69-3.71 GHz band after experiment.

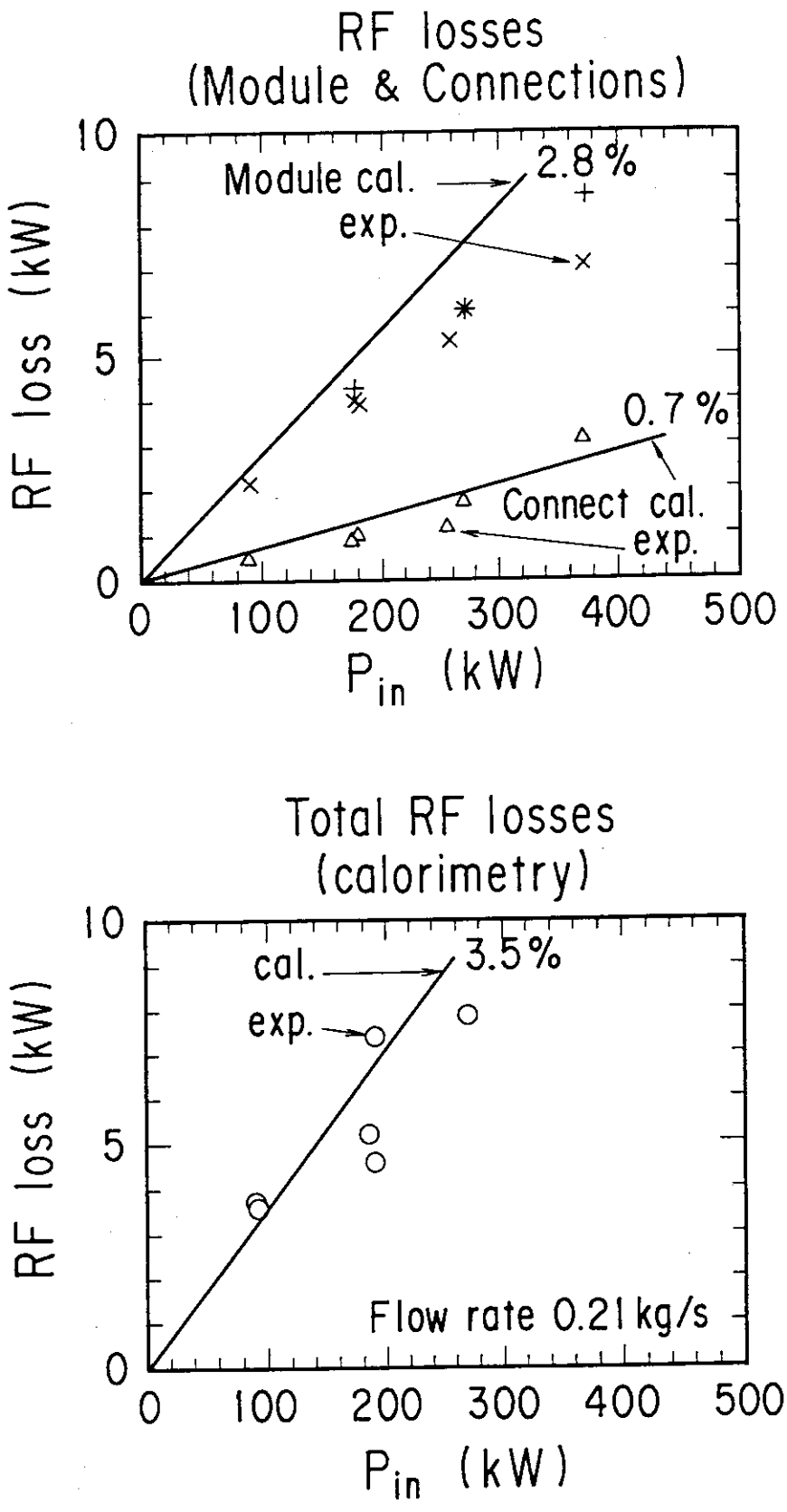

Fig. 23 a) Calculated and measured RF losses of the test module and the connection waveguides.

b) Calculated and measured given by calorimetry total RF losses.

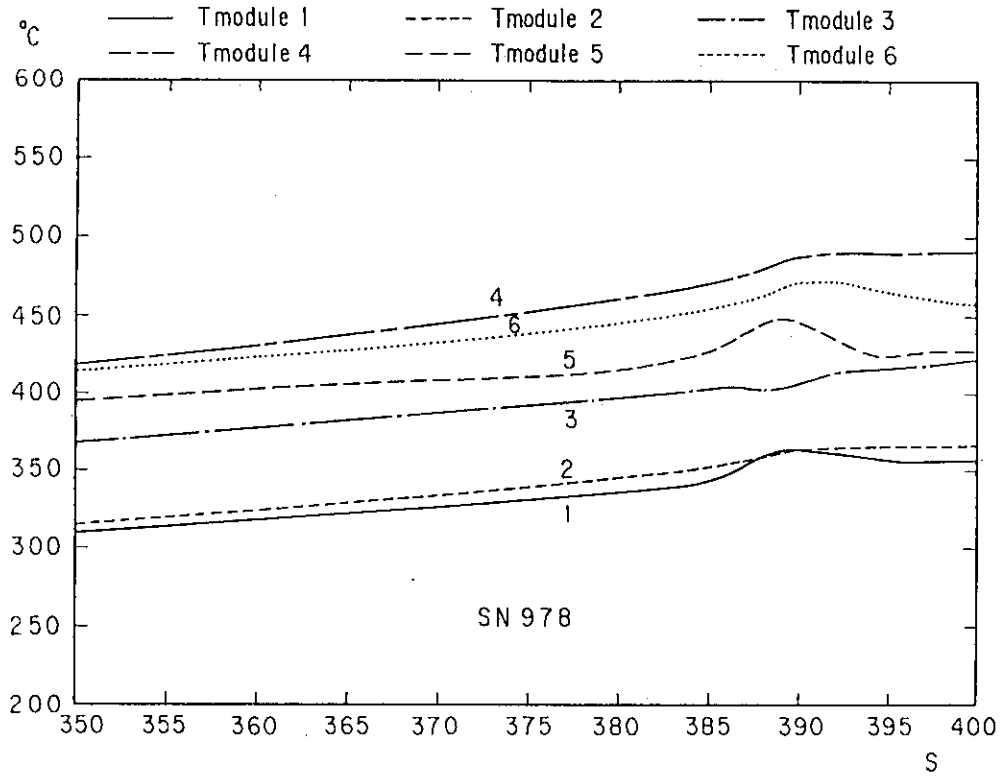

Fig. 24 Temperatures evolution during a shot when a resonance occurs.

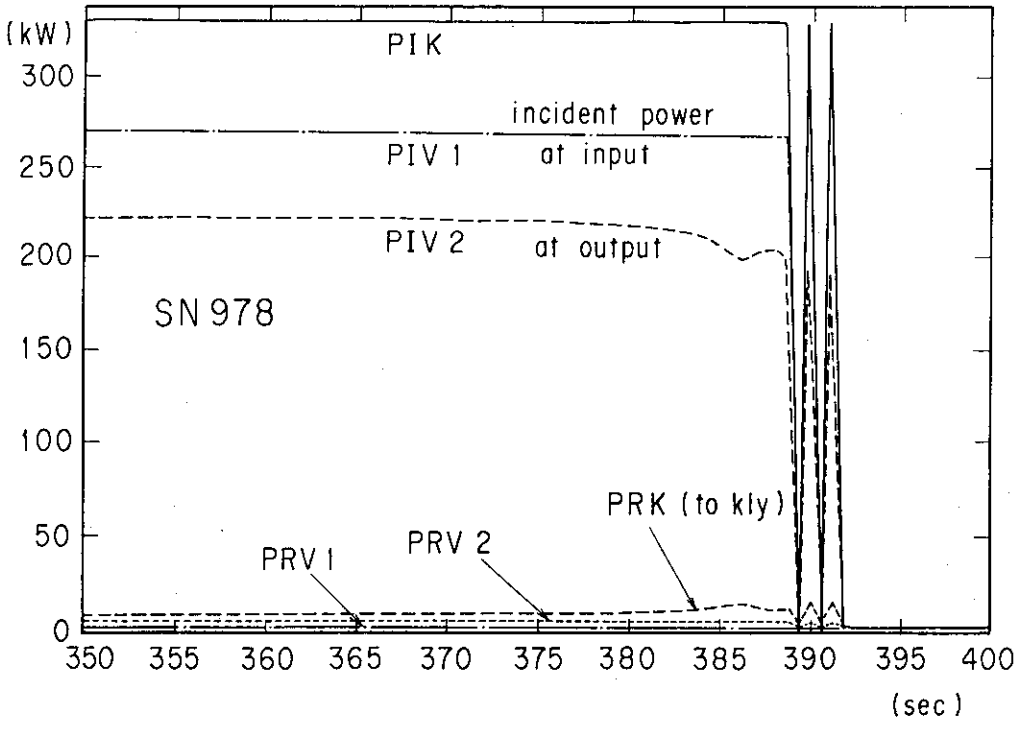

Fig. 25 RF measurements during the same shot as Fig. 24.

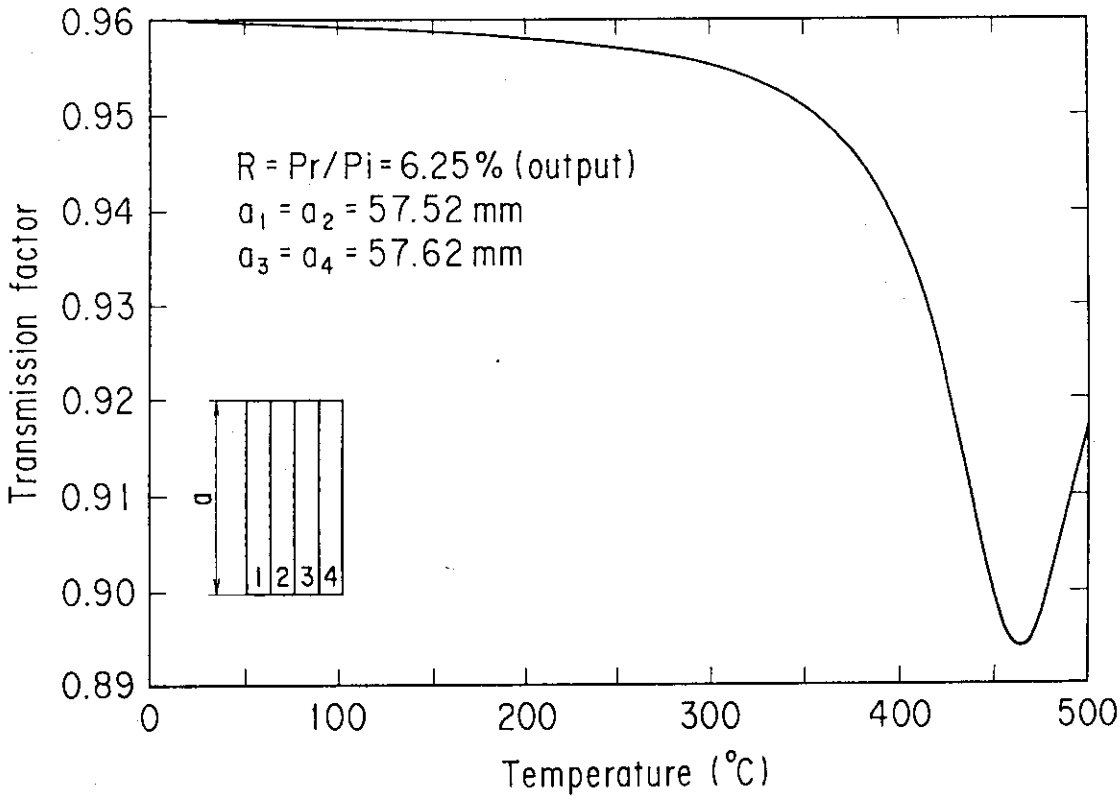

Fig. 26 Calculation of the power transmission coefficient assuming unbalanced height of the four waveguides.

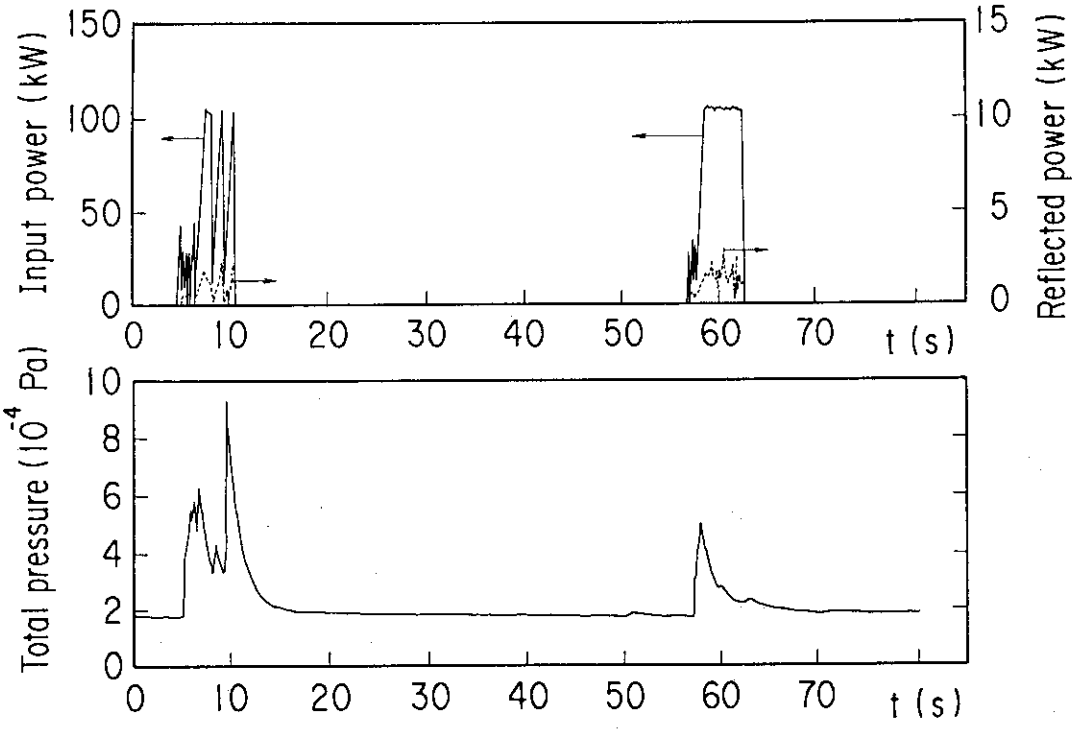

Fig. 27 First RF conditioning of the test module (incident/reflected powers and gas pressure) .

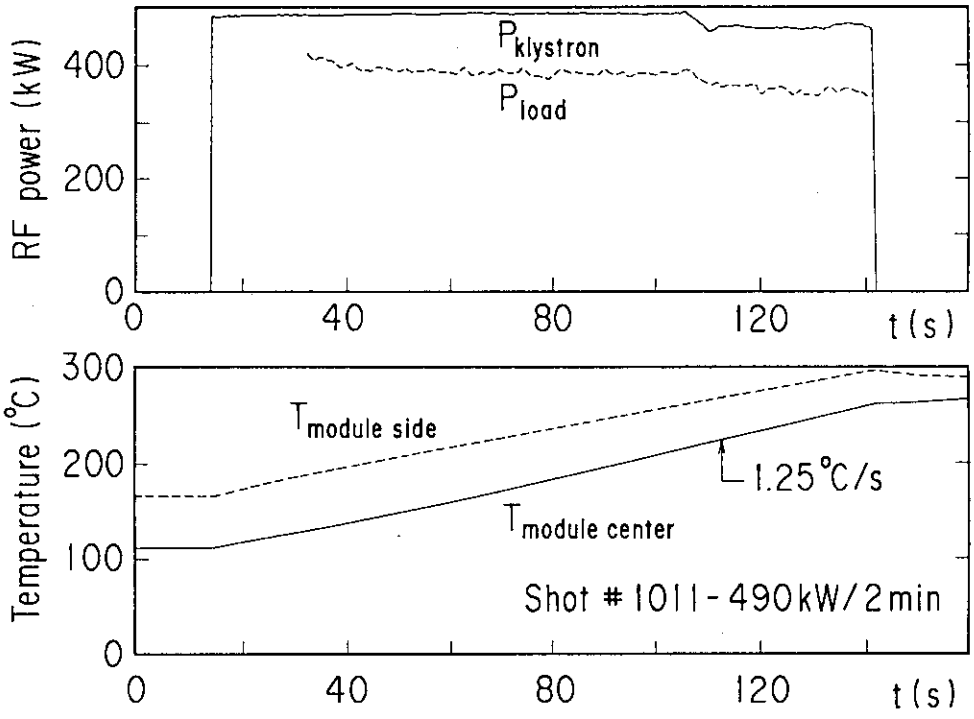

Fig. 28 RF injection at the 200 MW/m² level: incident power, power in the load and two module temperatures are shown.

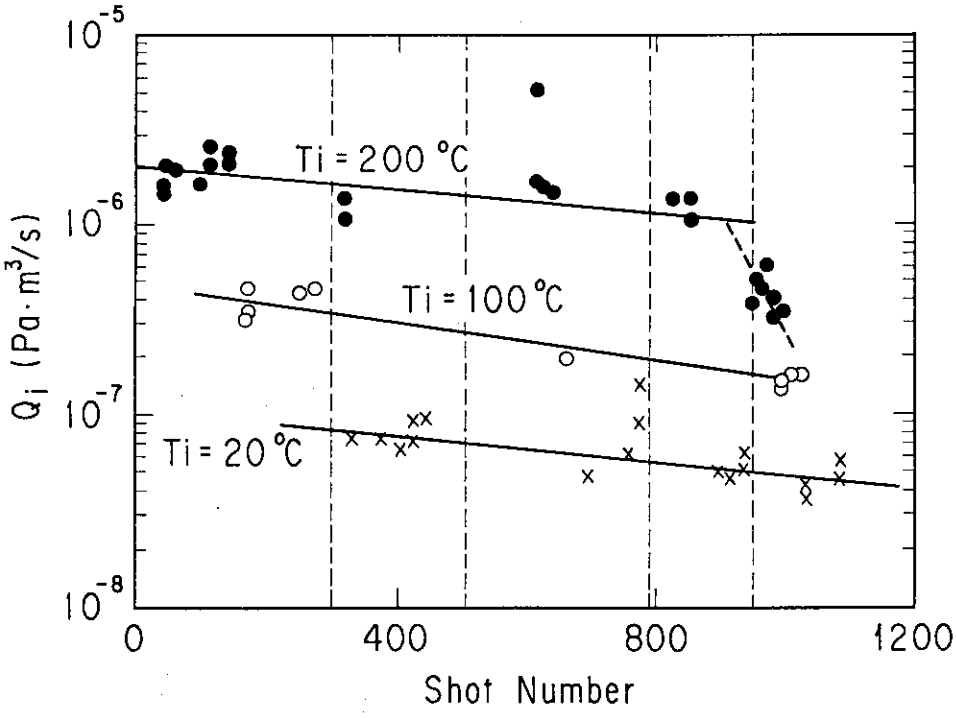

Fig. 29 Evolution of the total initial outgassing.

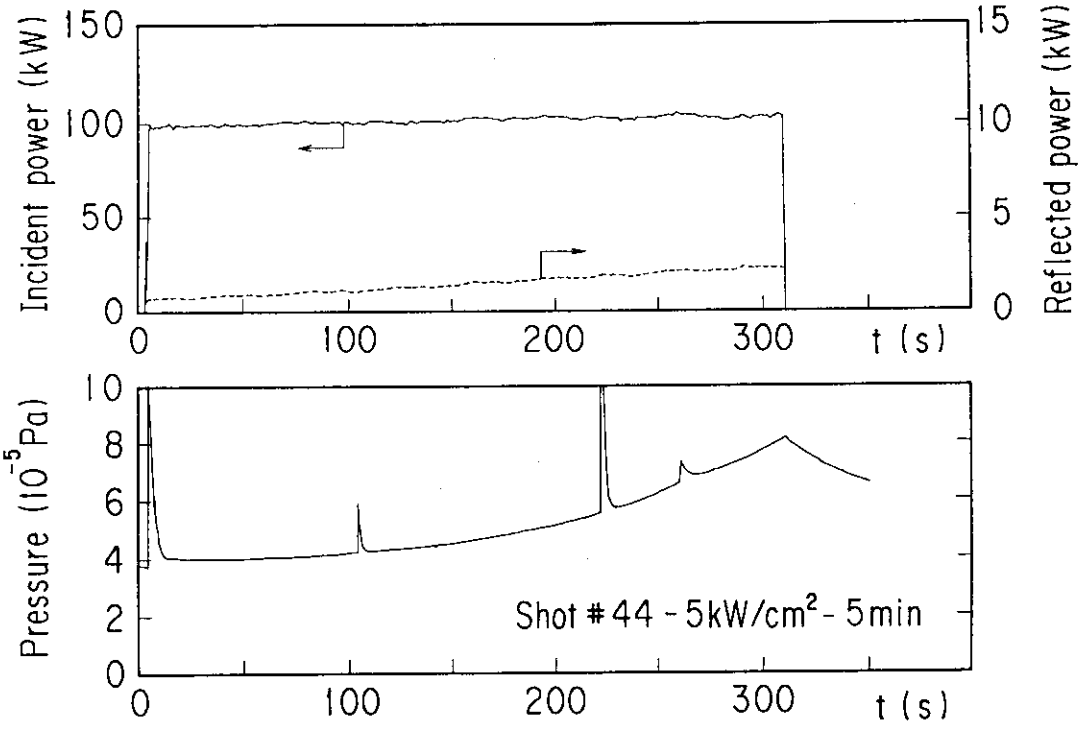

Fig. 30 First long shot 50 MW/m² level: incident/reflected powers and gas pressure are shown.

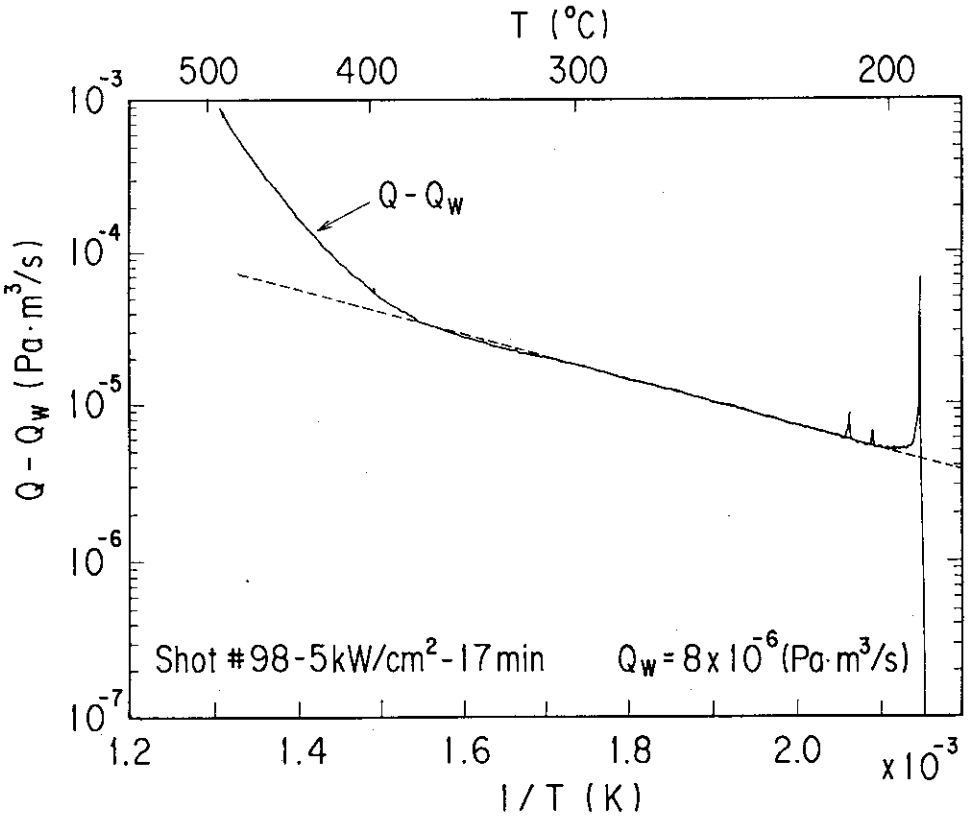

Fig. 31 Arrhenius plot of log Q vs 1/T for a 50 MW/m²-17 min shot.

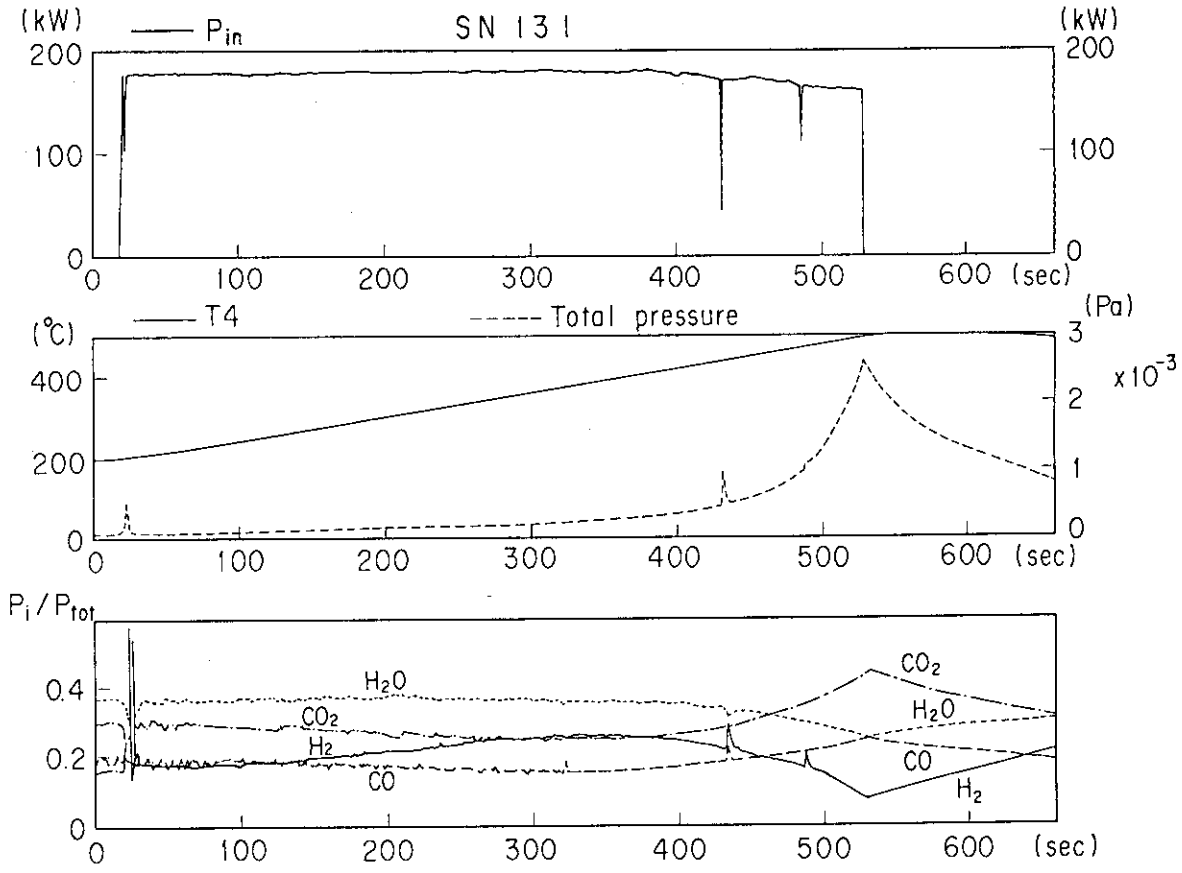

Fig. 32 Time evolution of gas composition during shot # 131.

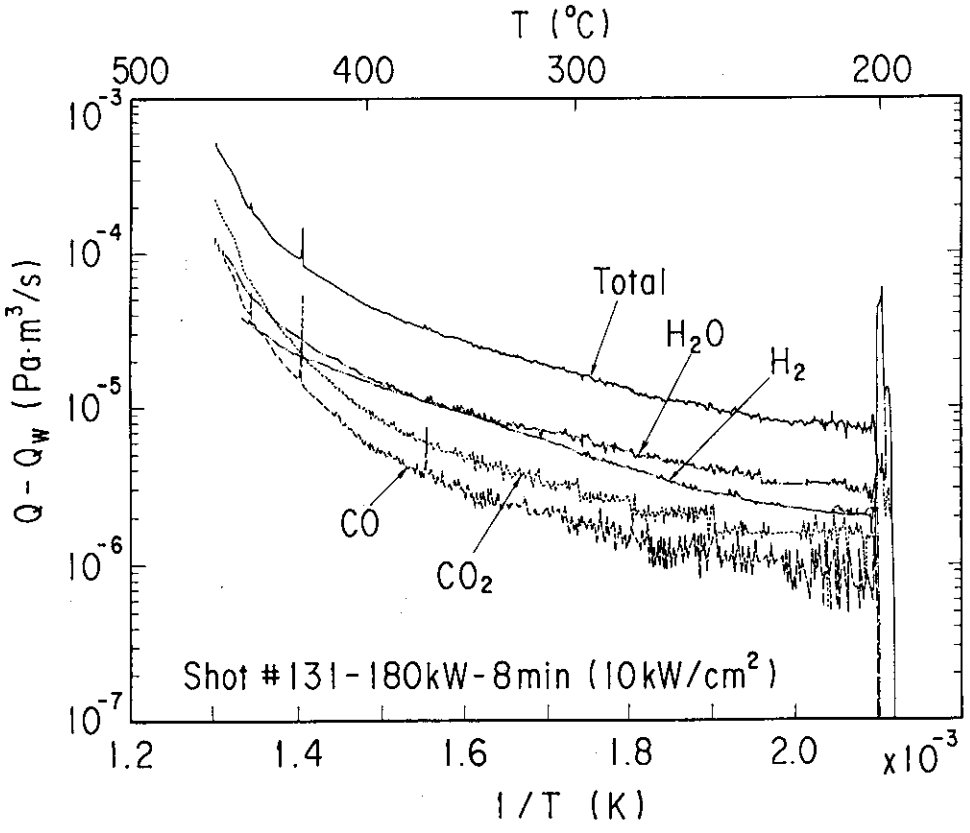

Fig. 33 Arrhenius plot for the four main outgassed species in shot # 131.

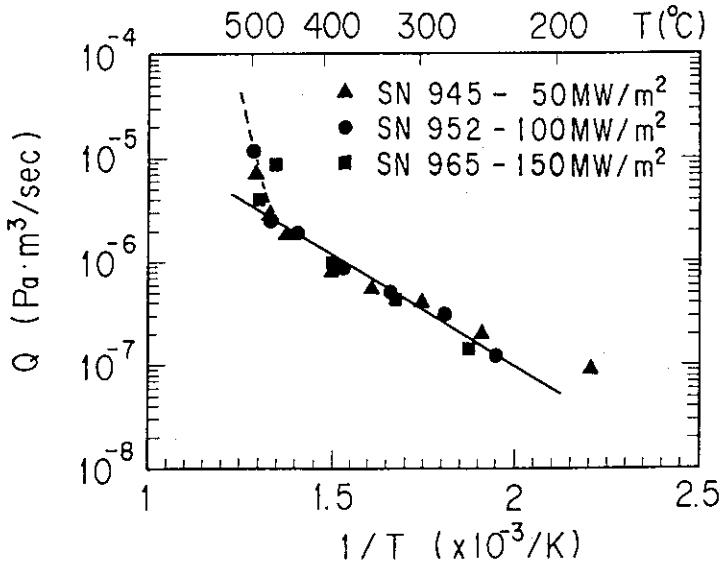

Fig. 34 Arrhenius plot for three shots at different power lovels.

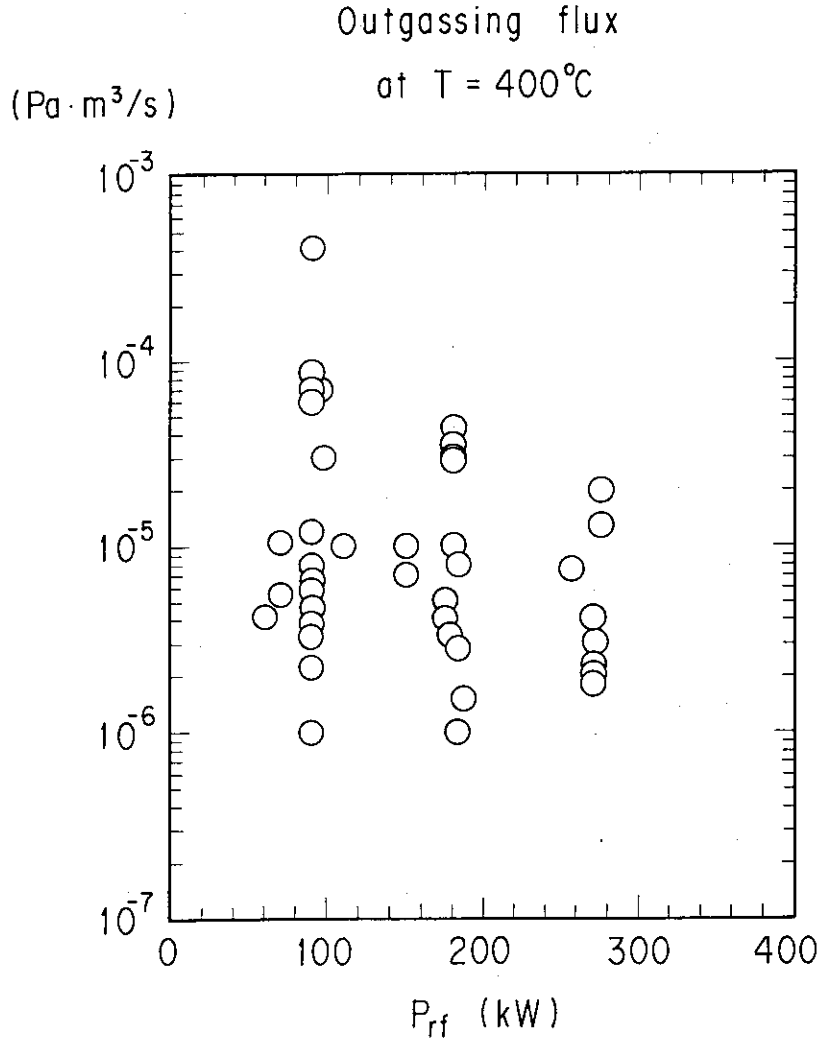

Fig. 35 Outgassing flux, at 400 ℃, as a function of the RF power.

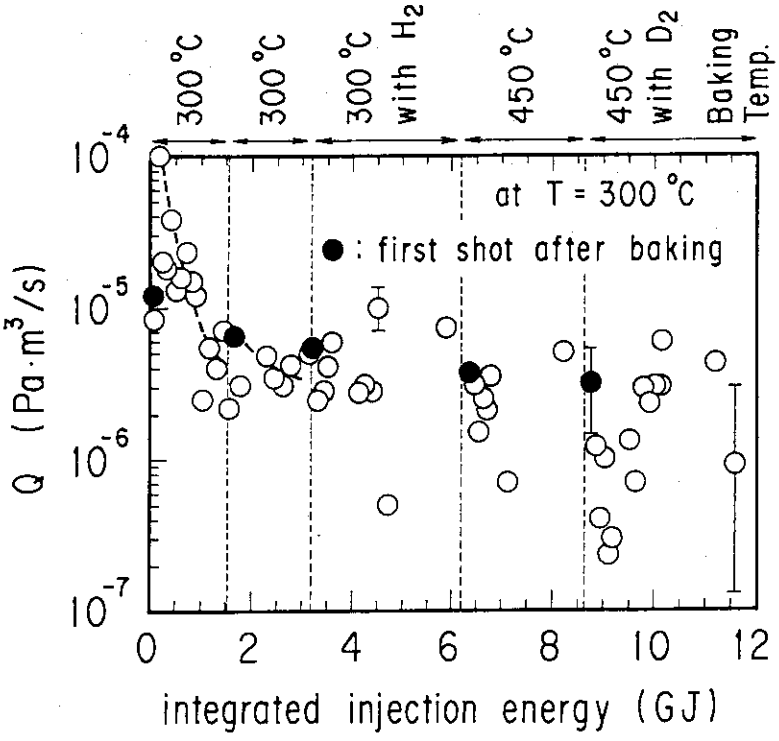

Fig. 36 Histogram of the outgassing flux at 300 ℃. Different baking treatments are indicated with a dashed line.

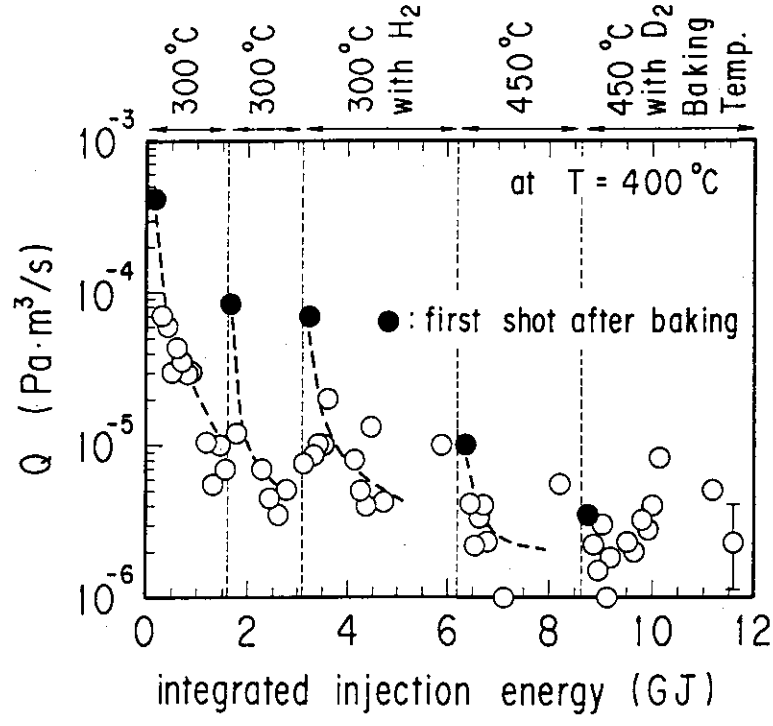

Fig. 37 Histogram of the outgassing flux at 400 ℃.

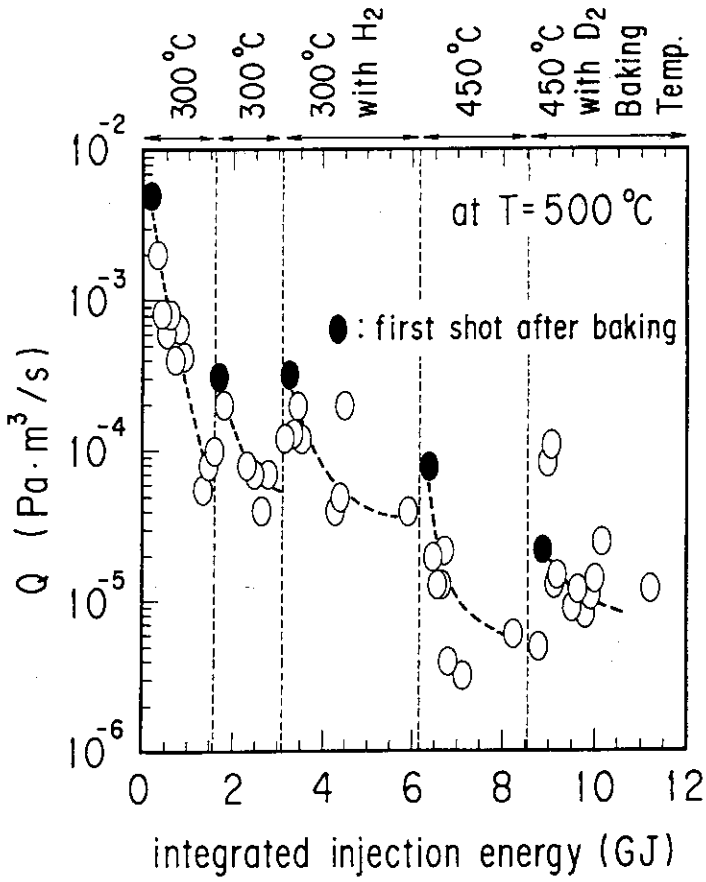

Fig. 38 Histogram of the outgassing flux at 500 ℃.

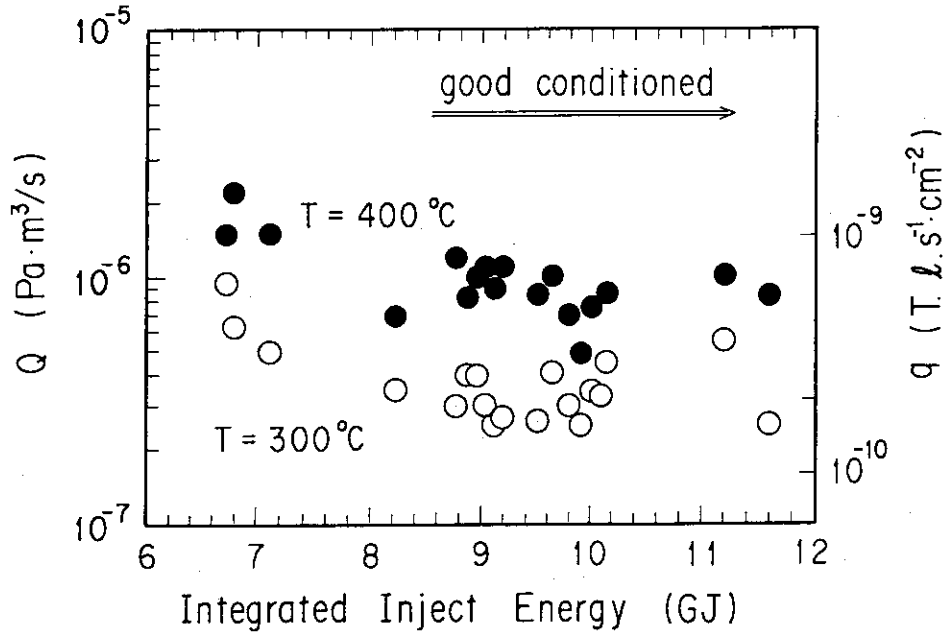

Fig. 39 Ultimate outgassing rate at T = 300 and 400 ℃.

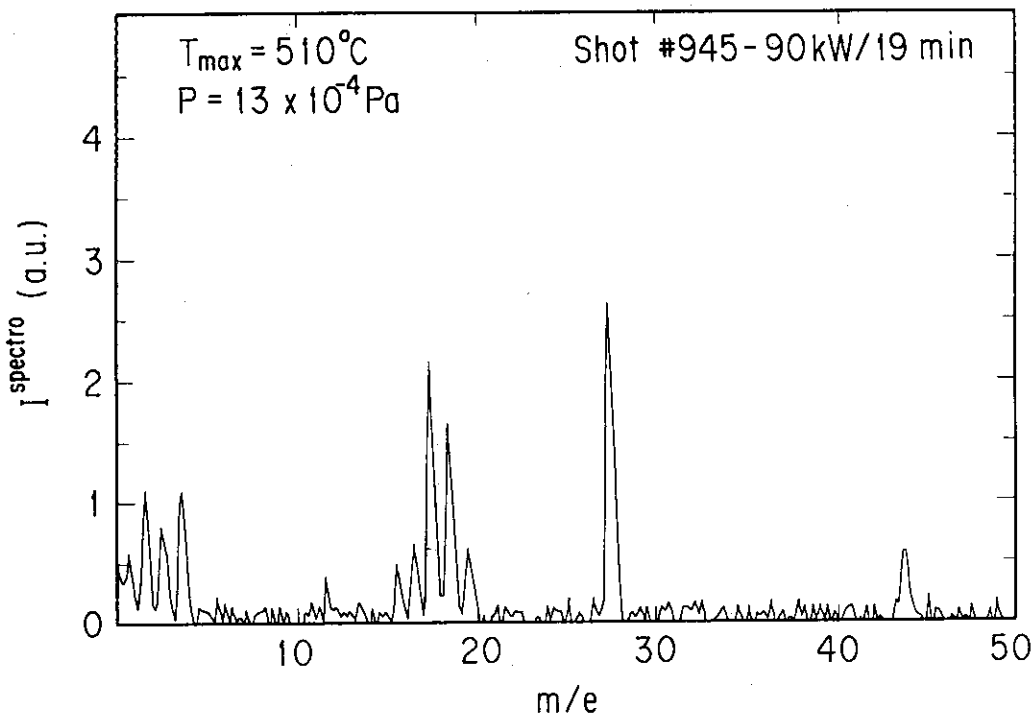

Fig. 40 Mass spectrum during RF injection after baking at 450 ℃ in deuterium atmosphere.

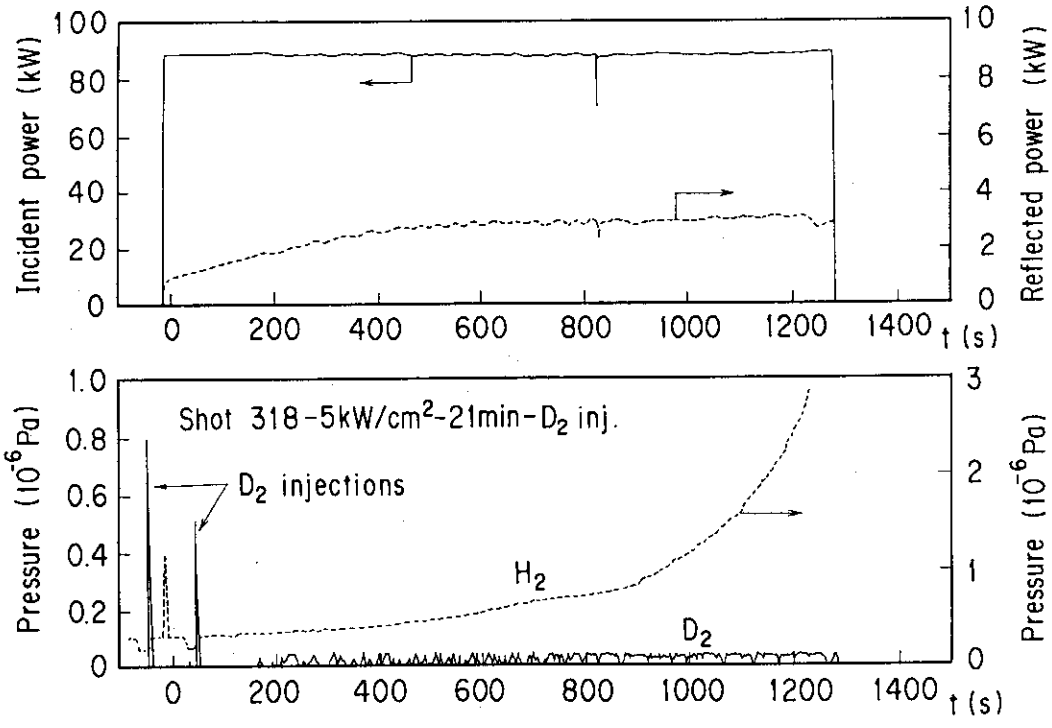

Fig. 41 Time evolution of H_2 and D_2 partial pressures after D_2 injections.

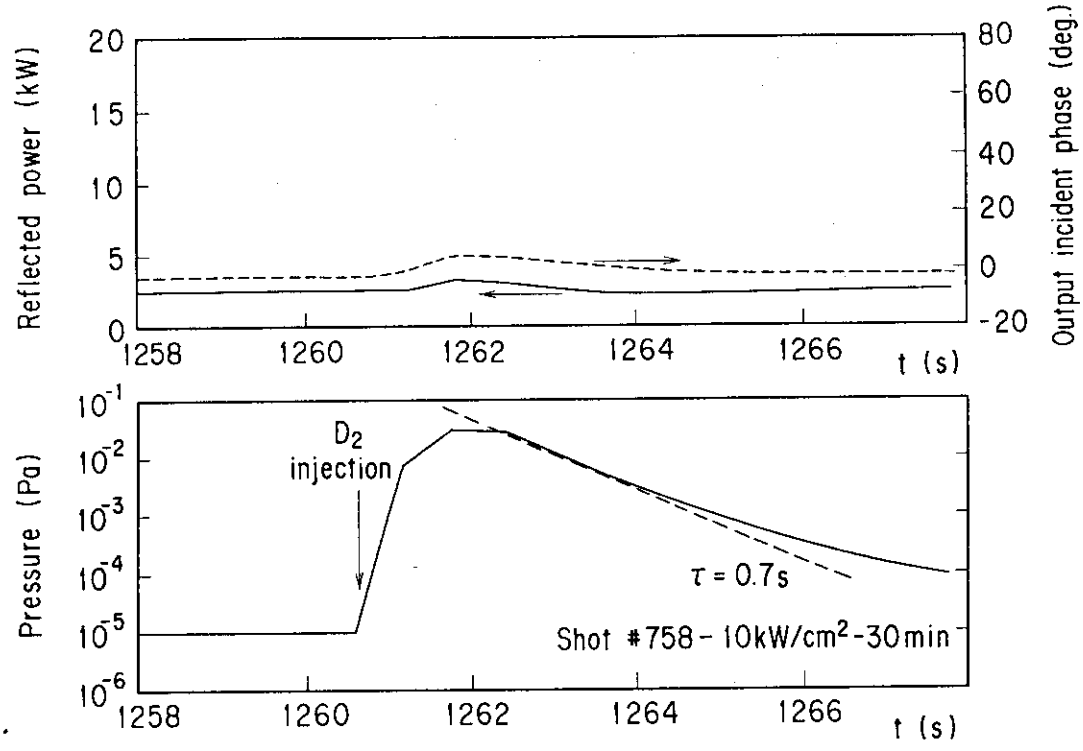

Fig. 42 Time evolution of the reflected power and the incident phase, at the output, during D_2 injection.

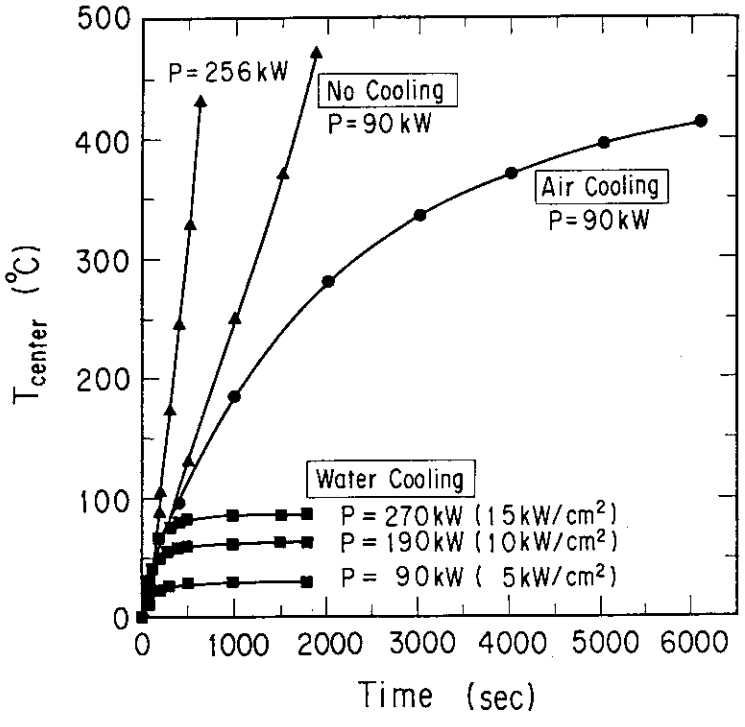

Fig. 43 Time evolution of the temperature at central part of the test module for different cooling.

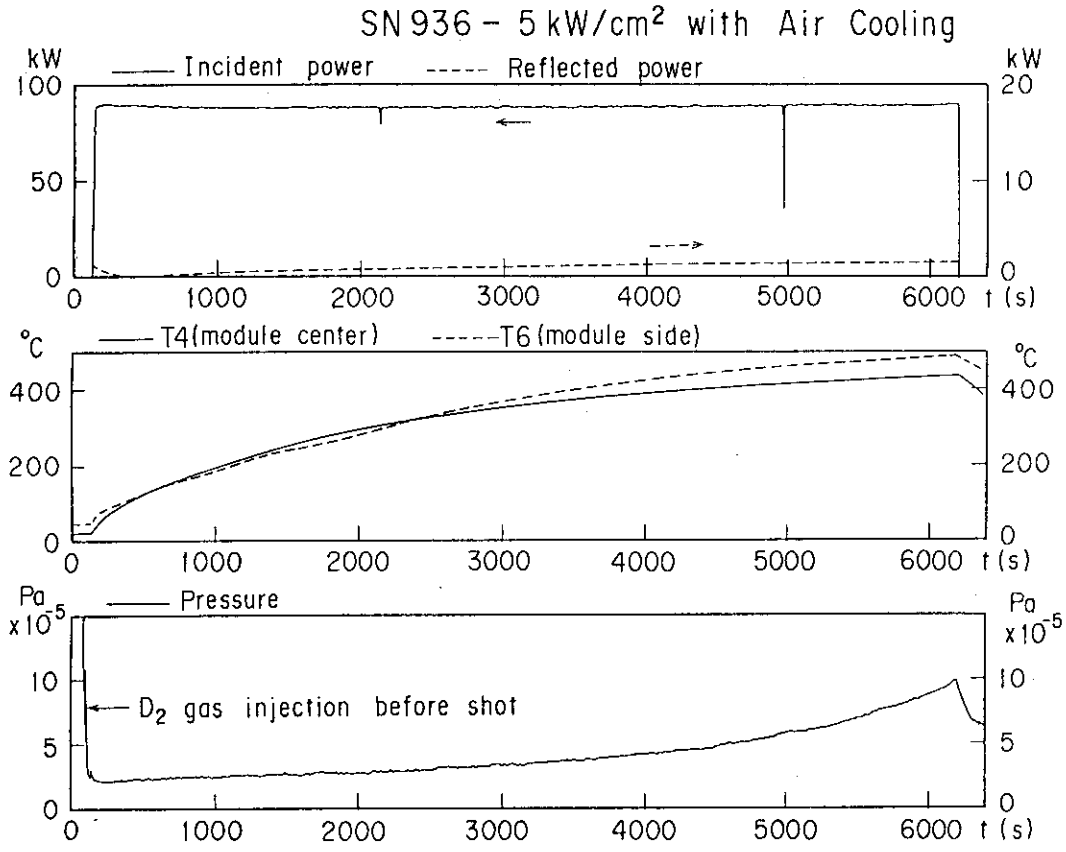

Fig. 44 Time evolution of the temperature and the pressure when the test module is air-cooled at shot # 936.

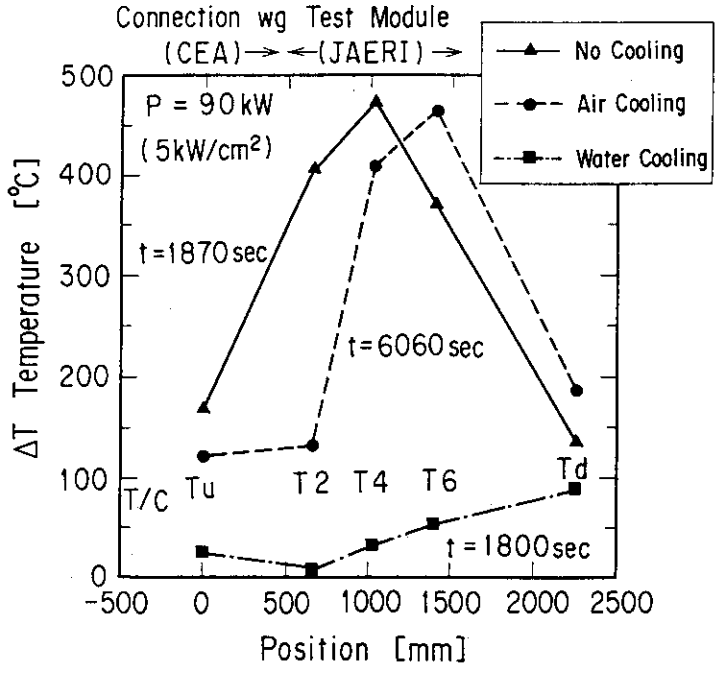

Fig. 45 Temperature profile for different cooling.

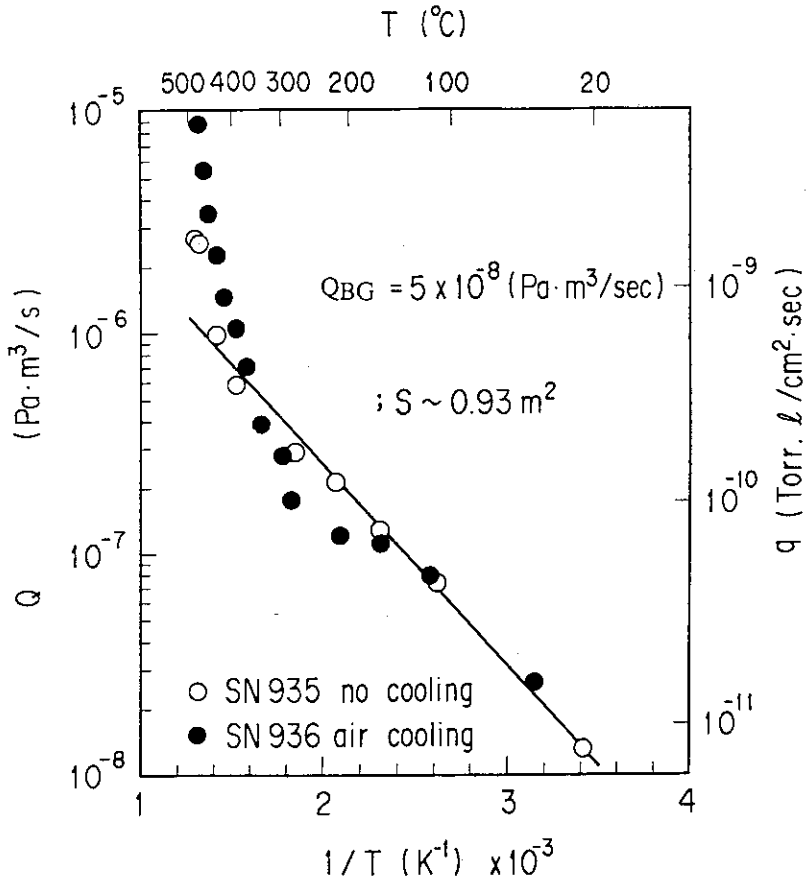

Fig. 46 Arrhenius plot for shot # 935 without cooling and shot # 936 with air-cooling.

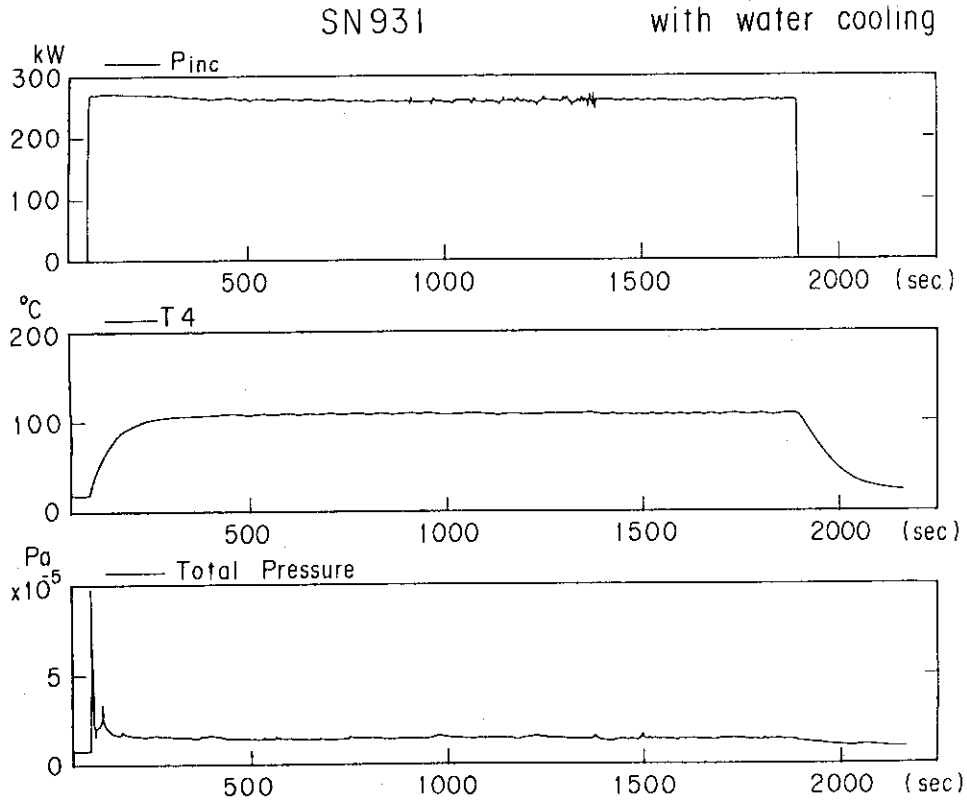

Fig. 47 RF injected power, the test module temperatures, pressure vs time in the case of water cooling.

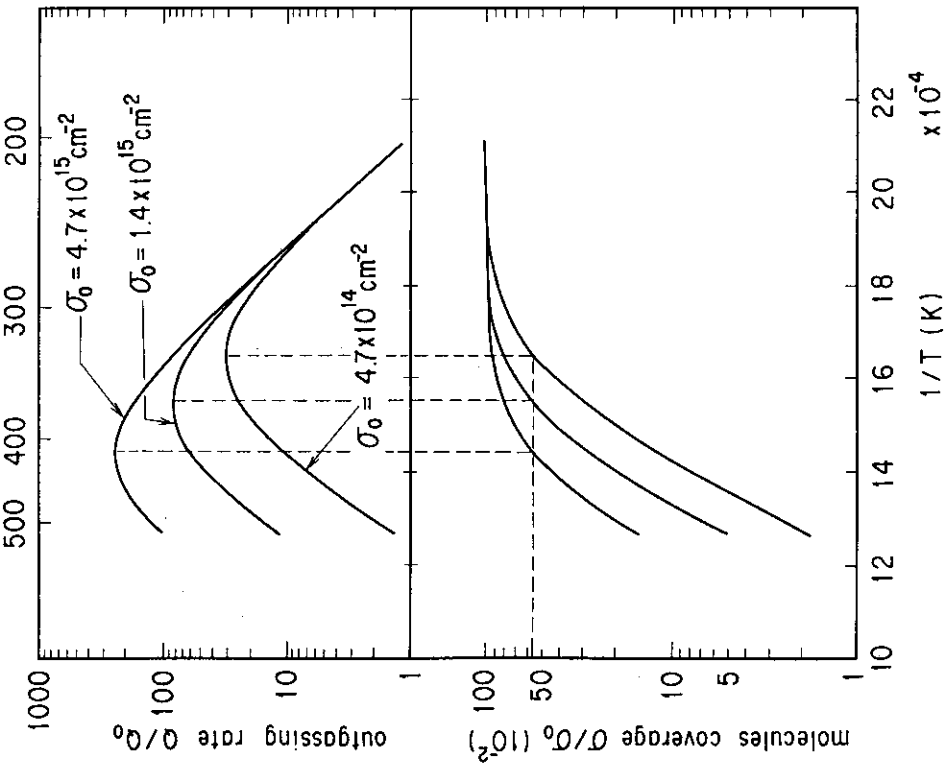

Fig. 48 Calculation of outgassing and molecules coverage vs 1/T for three cases of initial coverage $\sigma_0 = 1, 3, 10$ monolayers of H_2O ($T_0 = 202$ ℃, $Q_0 = 10^{-6}$ Pa m³/s m², b = 0.32K/s).

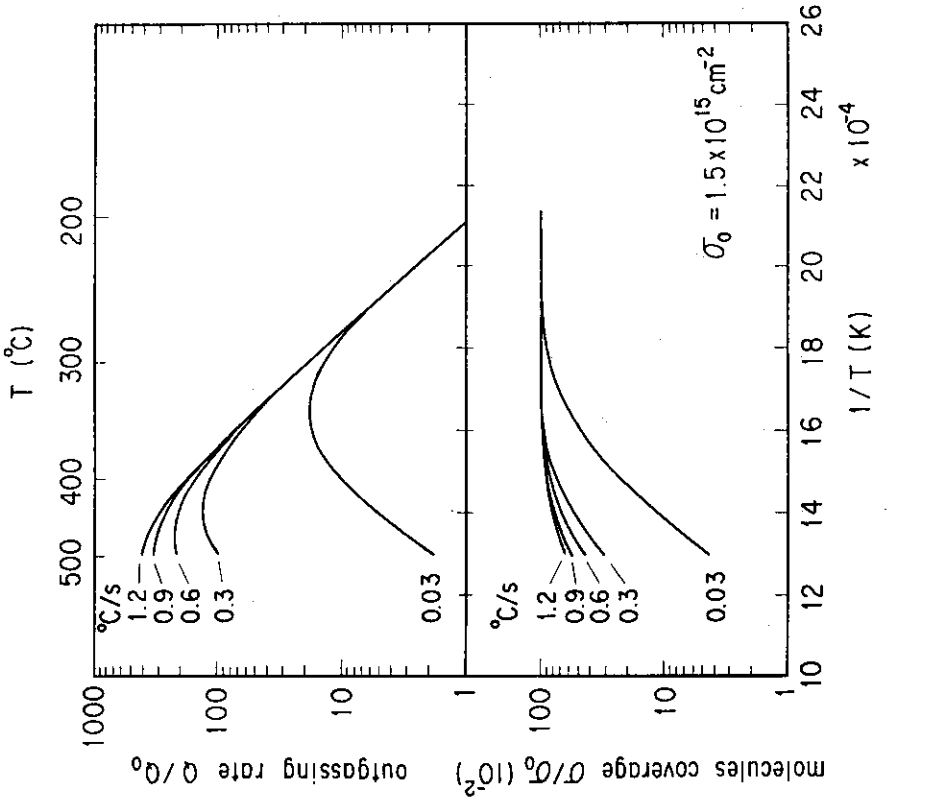

Fig. 49 Calculation of outgassing and molecules coverage vs 1/T for five cases of temperarure rise rate b = 0.03, 0.3, 0.6, 0.9, 1.2 K/s ($T_0 = 202$ ℃, $Q_0 = 10^{-6}$ Pa m³/s m², $\sigma_0 = 1.5\times10^{15}cm^{-2}$).

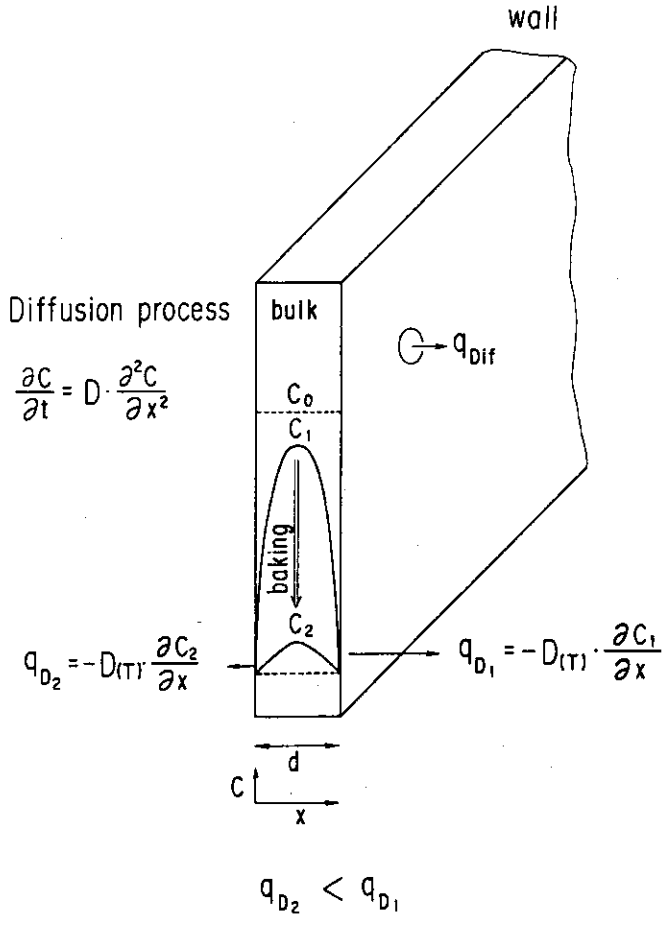

Fig. 50 Schematic explanation of baking effect on diffusion process.

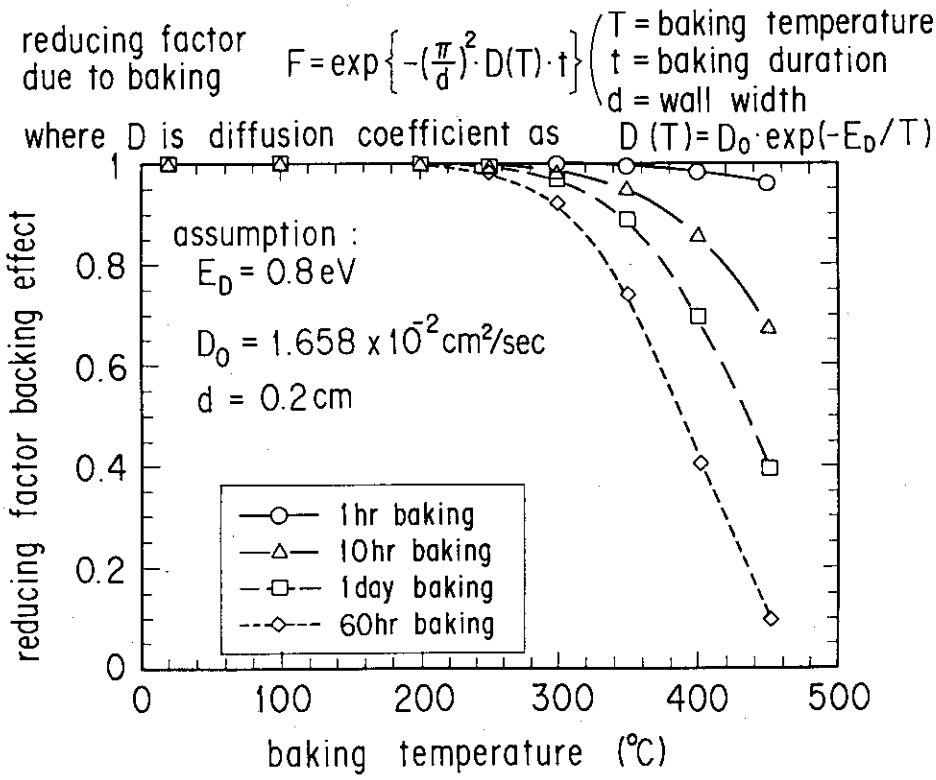

Fig. 51 The baking effect factor for a diffusion process.

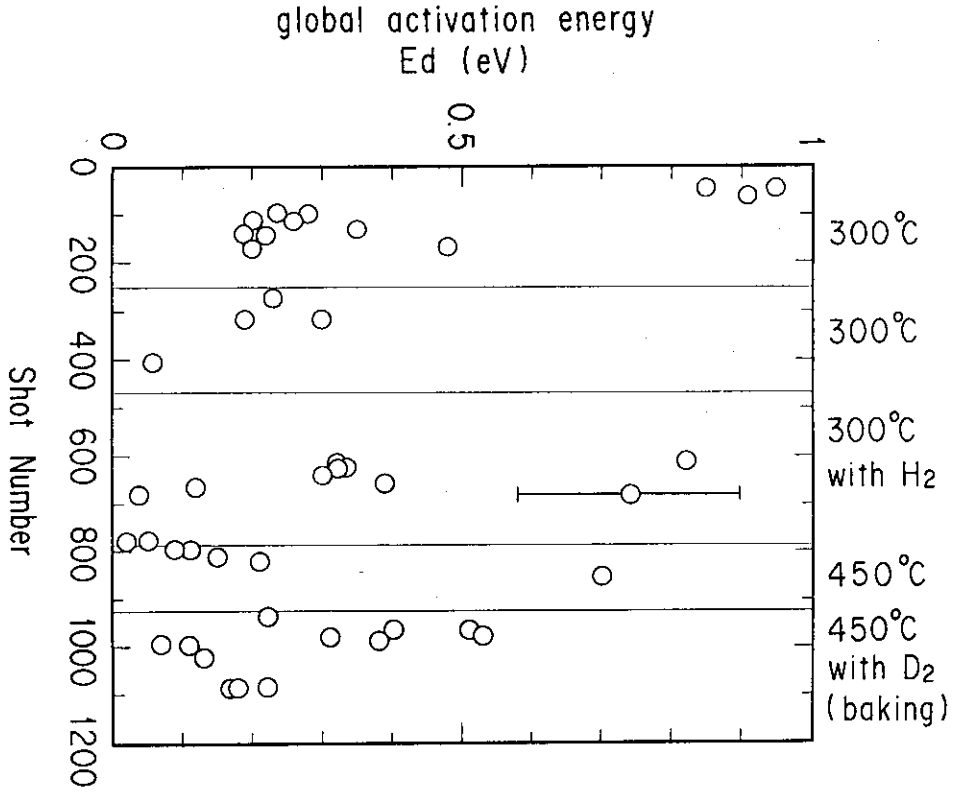

Fig. 52 Histogram of the global activation energy.

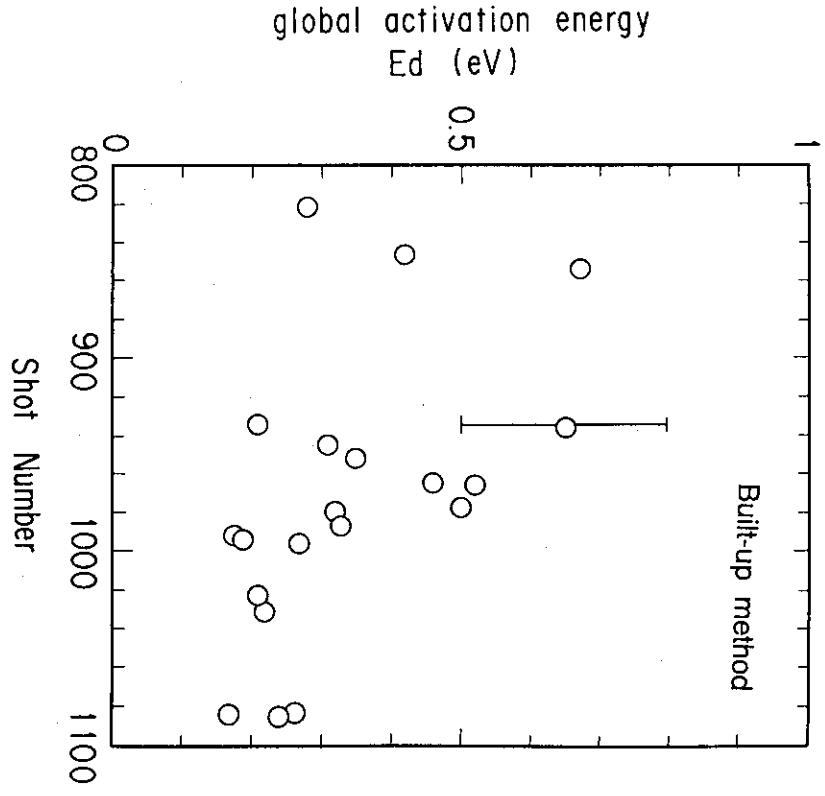

Fig. 53 Histogram of the global activation energy by build-up method.

Appendix 1

name	waveguides module	connection waveguide
material	wg : Cu-Al_2O_3 (flange:stainless steel)	wg : Cu-Zr (flange:stainless steel)
volume density ρ (x10^3 kg/m^3)	8.96 (7.8*)	8.96 (7.8*)
specific heat C_p (J/kg·K)	385 (460*)	385 (460*)
resistivity at 300°C η (10^{-8}Ω·m)	4.2	4.0
dividing number	divided into 4-waveguide	no (1-waveguide)
dimension axb (x10^{-4} mxm)	5.73 x 0.75	7.6 x 3.6
cross-section (x10^{-4} m^2)	17.2	27.4
length (m)	1.0	0.765 x 2-set
outgassing surface (m^2)	0.93	0.86
rf-loss surface (m^2)	0.52	0.35
Mass (kg)	18	16x2
rf-loss at 300°C (kW)	4.8**	1.4**
ΔT/Δt due to rf-loss at 300°C (K/sec)	0.68**	0.12**

Appendix 2

TEST BED FOR HIGH POWER TEST AT THE LOWER HYBRID FREQUENCY IN CADARACHE

1. TRANSMITTER

1.1. Klystron

Tube Thomson CSF TH2103
3.7 GHz +/- 5 MHz
450 / 500 kW, 210 s
Duty cycle at full power 1 / 3
Output power feedback controlled with an accuracy of +/- 2 % RF pulse shape can be changed :

- constant power with a ramp,
- sequence of short pulse.

(typically 10 ms every 100 ms).

1.2. Transmission line

Standard waveguides WR 284
Water cooled (Pmax = 6 bar)
Pressurized with SF_6 (Pmax = 1.3 bar).

1.3. RF load

Thomson-CSF
Water cooled
500 kW-CW.

1.4. RF measurements

Six power measurements
Two phase measurements.

2. HIGH VACUUM TANK

2.1. Dimensions

L x l x h = 2200 / 3200 x 140 x 250 mm
Volume : 0.142 m^3 (possible extension : 0.25 m^3)
Outgassing surface : 3.2 m^2 (possible extension : 4.7 m^2).

2.2. Pumping unit and gas injection

Turbo molecular pump of 0.5 m^3 / s, rotary pump of 0.33 m^3 / s
Gas injection system for H_2, Ar, N_2
Two BA. gauges, two Pirani gauges
Mass quadruple spectrometer (Balzers QMG 112).

2.3. Baking system

Bakable up to 450°C
Glow discharge cleaning (600 V - 15 A DC supply)
Six thermo-couples
Base pressure at 20°C : < 10^{-5} Pa.

2. 4. Cooling system

- water cooling (P = 6 bar)
- air cooling 50 N m^3 / hr

2.5. Flanges

Flange supporting the RF window using Viton O-ring : bakable up to 150°C
Feedthroughs (ϕ = 16, 32, 64)
Flange (ϕ = 32) for four thermo-couples
Twelve view ports (ϕ = 32).

3. CONTROL AND DATA ACQUISITION

3.1. Klystron control

Controlled by a wired electronics.

3.2. Data acquisition

- desk computer equipped with two cards of 64 channels each (fast and slow acquisition rate),
- quadruple data processor (Balzers QDP 101) for partial pressure.

Appendix 3

< stage 1 >
power capability test
achieved power level : 50 MW / m^2 - 6s
< stage 2 >
thermal treatment #1
- temperature : 300°C
- duration : 60 hours

achieved power level : 100 MW / m^2 - 9 min
< stage 3 >
thermal treatment #1' (after air keak)
- temperature : 300°C
- duration : 60 hours

achieved power level : 150 MW / m^2 - 10 min
< stage 4 >
thermal treatment #2
- temperature : 300°C
- duration : 50 hours

gas treatment
- temperature : 300°C
- duration : 10 hours
- working gas : Hydrogen of 10 Pa

< stage 5 >
thermal treatment #3
- temperature : 400°C
- duration : 45 hours

+
- temperature : 450°C
- duration : 10 hours

< stage 6 >
thermal treatment #4
- temperature : 400°C
- duration : 50 hours

gas treatment
- temperature : 450°C
- duration : 8 hours
- working gas : Deuterium of 10 Pa

< stage 7 >
power capability test
achieved power level : 200 MW / m^2 - 2 min